

Tunneling of quantum rotobreathers

J. Dorignac, S. Flach

Max-Planck-Institut für Physik komplexer Systeme, Nöthnitzer Straße 38, D-01187 Dresden

(Dated: October 24, 2018)

We analyze the quantum properties of a system consisting of two nonlinearly coupled pendula. This non-integrable system exhibits two different symmetries: a permutational symmetry (permutation of the pendula) and another one related to the reversal of the total momentum of the system. Each of these symmetries is responsible for the existence of two kinds of quasi-degenerated states. At sufficiently high energy, pairs of symmetry-related states glue together to form quadruplets. We show that, starting from the anti-continuous limit, particular quadruplets allow us to construct quantum states whose properties are very similar to those of classical rotobreathers. By diagonalizing numerically the quantum Hamiltonian, we investigate their properties and show that such states are able to store the main part of the total energy on one of the pendula. Contrary to the classical situation, the coupling between pendula necessarily introduces a periodic exchange of energy between them with a frequency which is proportional to the energy splitting between quasi-degenerated states related to the permutation symmetry. This splitting may remain very small as the coupling strength increases and is a decreasing function of the pair energy. The energy may be therefore stored in one pendulum during a time period very long as compared to the inverse of the internal rotobreather frequency.

PACS numbers:

I. INTRODUCTION

As revealed by the increasing number of recent papers [1]-[26], the quantum counterpart or the quantization of classical discrete breathers (CDBs) has become these very last years a real challenging and exciting field. At present, indeed, the theory of CDBs, i.e. "time-periodic spatially localized motions in networks of oscillators (MacKay [23])", has reached a high degree of perfection and may certainly be considered as a real achievement. As it is well known, the necessary condition required for a Hamiltonian lattice to support such CDBs is that the breather frequency as well as its harmonics do not lie inside the phonon band. Such a non resonance condition may be achieved by the interplay of discreteness and nonlinearity, the first providing a natural upper bound of the linearized Hamiltonian spectrum (say phonons) whereas the latter allowing for a tuning of frequencies out of this spectrum [27].

Mathematical existence proofs of CDBs have been obtained for a wide variety of model Hamiltonians [28] and have simultaneously given rise to an accurate numerical method allowing for their practical construction [29]. Both are based on the so-called *anti-continuous* limit (i.e. the limit where the coupling between oscillators vanishes), provided a nonlinear onsite potential is present. In this limit time-periodic spatially localized (on one or more sites) solutions trivially exist. More recently, an existence proof of CDBs based on a discrete version of the center manifold reduction has also been given for the FPU chain for which the method based on the anti-continuous limit fails [30]. This completes and enlarges the results previously obtained in [31] by a homoclinic orbit approach. At last, also recently, a variational approach has been carried out to prove the existence of hard

discrete breathers in some classes of Hamiltonians [32]. Obviously, the wide range of applications of these rigorous mathematical results supports the idea that CDBs are generic solutions of nonlinear Hamiltonian lattices as claimed for the first time by Sievers and Takeno in 1988 when they discovered this new kind of intrinsic localized modes [33].

Together with their existence proofs, the properties of CDBs have been extensively studied. It has been shown for example that they are structurally stable provided the non resonance condition holds [27] and linearly stable in any dimension provided the coupling is weak enough [14]. Their spatial decay is generally exponential (for any finite range interaction potential) but may be also algebraic in case the interaction potential itself is algebraically decaying [34]. More recently, it has even been confirmed that a pure nonlinearity of the interaction potential may give rise to a super-exponential decay of the breather tail [27, 35]. At last, and directly related to their spatial decay properties, possible energy thresholds for their appearance have been derived according to whether the lattice dimension exceeds a system-dependent critical value or not [36]. Extensive studies of CDBs properties as well as the perspectives in this field may be found in different reviews (see for instance [14, 15, 23, 25, 37]).

The general properties of CDBs briefly listed above shows how well their theory is understood at present. Much less is known on the other hand about their quantum counterparts (QDBs), that is, about the quantum states which would behave similarly to CDBs in a sense to be clarified below. Nevertheless, this question is of great importance given one natural area of application, namely, the condensed matter physics where quantum effects have generally to be considered (see [23] and refs. therein for a review of the materials where the presence of DBs is suspected, expected or has been detected). This is

the precise reason why the quantum theory of breathers is currently in full development.

Let us turn back to an essential property of CDBs. These time-periodic solutions occur in a lattice but are spatially localized which means that they are not invariant under the discrete translational symmetry of the lattice whereas the Hamiltonian does. If we now consider the corresponding quantum problem, the invariance of the quantum Hamiltonian \hat{H} with respect to the discrete translational symmetry (the operator of which we denote by \hat{T}) yields $[\hat{H}, \hat{T}] = 0$. The eigenstates of \hat{T} are thus eigenstates of \hat{H} and are delocalized along the lattice (Bloch waves). Of course, this discrete translational symmetry of the lattice is broken if we consider for instance a finite system with fixed or open boundary conditions. Nevertheless, if the lattice consists of a sufficiently large number of sites, discrete translational symmetry is practically restored similar to the infinite lattice. However, at large enough energy the quantum and the classical descriptions of the system should give similar results!

It is possible to reconcile the quantum and the classical points of view provided we again start from the anti-continuous limit. In this limit indeed, the Hamiltonian consists only of a sum of identical Hamiltonians (one for each site) $\hat{H} = \sum_s \hat{H}_s$ and a general eigenstate $|\psi\rangle$ of the system may be represented as the tensorial product of local eigenstates $|\phi_s\rangle$, $|\psi\rangle = \otimes_s |\phi_s\rangle$. Then, a localized excitation is obviously constructed by creating an excitation of level k at site n , $|\phi_n^{(k)}\rangle$ whereas the other sites reside in their ground state $|\phi_{s \neq n}^{(0)}\rangle$. This leads to $|\psi_n^{(k)}\rangle = \otimes_{s < n} |\phi_s^{(0)}\rangle \otimes |\phi_n^{(k)}\rangle \otimes_{s > n} |\phi_s^{(0)}\rangle$. This case corresponds to the classical one used to initialize the construction algorithm of a CDB at non zero coupling. Nevertheless, any eigenstate of the form $|\psi_j^{(k)}\rangle = \otimes_{s < j} |\phi_s^{(0)}\rangle \otimes |\phi_j^{(k)}\rangle \otimes_{s > j} |\phi_s^{(0)}\rangle$ has the same energy. The corresponding eigen-subspace has a dimension N equal to the number of sites (provided no additional accidental degeneracy occurs). Therefore in the uncoupled (anti-continuous) limit, any unitary transform of the preceding basis leaves the subspace invariant although it yields a new basis. As the Hamiltonian system is invariant under the discrete translation \hat{T} whatever the intersite coupling ε is, at non zero coupling, the eigenstates of \hat{H} must belong to one of the N symmetry sectors defined by \hat{T} . When the coupling becomes zero, we may thus choose the eigenbasis of \hat{T} as a basis of the N -dimensional subspace. We denote its eigenvectors by $|\lambda_q^{(k)}\rangle$ where q labels the symmetry sector. Of course each of these new eigenstates is completely delocalized (in the sense that $\forall q, [\sum_j |\langle \psi_j^{(k)} | \lambda_q^{(k)} \rangle|^4]^{-1} = N$).

Let us assume now that we switch on the coupling between the sites. We expect the N -fold degenerated eigenenergy to be splitted under the effect of the perturbation and to form a band of N nearly degenerated eigenenergies. The corresponding eigenstates, which already had the correct symmetry because of the unitary

transform \hat{T} performed on the local basis at $\varepsilon = 0$, now give a new (perturbed) basis $|\lambda_q^{(k)}(\varepsilon)\rangle$. Provided ε is weak enough, these new eigenvectors are close to those defined at the uncoupled limit and thus an inverse unitary transform \hat{T}^{-1} is expected to yield a basis $|\psi_n^{(k)}(\varepsilon)\rangle$ close to the local basis of the uncoupled limit, that is, $|\psi_n^{(k)}(\varepsilon)\rangle = |\psi_n^{(k)}\rangle + \mathcal{O}(\varepsilon)$. These states are thus well localized provided the coupling is weak enough. However, being a linear combination of non degenerated eigenstates, they are no more eigenstates of \hat{H} and evolve in time. This tunneling effect, corresponding to the transfer of an initial excitation from site to site, takes a time typically given by the width of the band at a given value of the coupling ε . In order to gap the bridge between the classical manifestation of the breather solution and its quantum realization, we thus expect the quantum system to exhibit bands of N nearly degenerated eigenstates whose width tends to zero as the average energy of the band goes to infinity.

The purpose of a quantum theory of breathers is thus to know how the above defined bands behave as the coupling increases. Several successful attempts to answer this question have already been done in one-dimensional systems which present the particularity to be integrable ([4], [6]-[11] and the review [22]). The (soliton/breather) bandwidth is shown to behave typically like $\Delta E_n \sim (\varepsilon/\gamma)^n / (n-1)!$ where n is strictly speaking the number of bosons in the system. This number corresponds to the number of the excited level of a single site in the absence of interaction $\varepsilon = 0$ and typically depends on energy as a power law. Finally γ is a measure of the onsite (quartic) nonlinearity. It is then obvious that for bands of high energy ($n \rightarrow \infty$), the bandwidth goes rapidly (in fact more than exponentially fast) to zero with increasing n . In this case the tunneling time goes to infinity in the classical limit and the quantum breather (quasi-classical) state remains localized on its initial site.

Several questions remain however. At high energy, if the onsite potential behaves like x^{2q} , the density of states (evaluated at $\varepsilon = 0$ by the mean of the Weyl's formula) scales like $g(E) \sim E^{N(1+q)/(2q)-1}$ as $E \rightarrow \infty$, where N is the number of sites. An immediate conclusion is that if the number of sites is greater or equal to 2, the density of states (DOS) increases with energy according to a power law with exponents linearly depending on N . Then, we may ask whether the corresponding raise of interaction possibilities (hybridization) will destroy the quantum breather bands or not. A partial answer to this question should be given by the ratio of the breather bandwidth and the mean level spacing $1/g(E)$ at a given (high) energy E : $\lim_{E \rightarrow \infty} g(E)\Delta E$? Assuming that the DOS scales as indicated by the Weyl's formula, the ratio of the bandwidth to the mean level spacing will tend to zero provided the bandwidth decreases exponentially with increasing energy (or faster). The above mentioned integrable examples fall into this category. This result seems to indicate and to explain the possibility, starting from the quantum problem, to recover the limit of the

classical breather at high energy. Another natural question is related to the impact of the nonintegrability of the system on the quantum breather bands and in particular the influence at the quantum level of the chaotic trajectories induced by the nonintegrability lying nearby the classical breathers.

Up to now, except for integrable systems, where analytical results are obtainable, studies of quantum breathers have been done numerically. Such studies become rapidly extremely difficult due to the huge matrices to be diagonalized and so far have been restricted to small 1D systems for which the number of sites has not exceeded $N = 12$ [20]. Even for these moderate lattice sizes, the average dimension of the (truncated) Hamiltonian matrices is generally of order 10^6 and requires specific numerical diagonalization methods [13, 16]. The numerical results reported in the papers mentioned above are restricted to the low energy sector as soon as the number of sites exceeds a few units. This is easily understood given the number of configurations obtainable by truncating the basis to p bosons per sites on N sites $((p + 1)^N)$. Remains the possibility to study very small systems ($N = 2$ or 3), as it has already been done for the dimer (integrable) [4, 12] and the trimer (non integrable) [24, 55]. The dimer has also been used to describe the tunneling of a QB along a chain by a suitable linearization of the lattice around it [18]. This linearization method was also employed to study the properties of classical rotobreathers in a chain of pendula [52]. But the specific properties of quantum rotobreathers have not been discussed yet. We will consider a dimer of two coupled quantum pendula which, due to the presence of both nonlinear onsite and interaction potentials, is not integrable.

As far as we know, no experimental study of quantum rotobreathers has been done yet. This is possibly due to their quite large activation energy. The reader should notice however that a large number of studies have been devoted to the rotational motions of molecules (see e.g. [38, 39, 40, 41]) especially concerning the methyl groups whose dynamical properties are usually obtained via neutron scattering [3, 5, 17, 42, 43]. But the transitions thus obtained concern the so-called quantum rotational tunneling effect [43]. This tunneling occurs between the equilibrium positions defined by the onsite potential which is n -fold according to the individual symmetry of the observed molecule and the symmetry of its environment. For the methyl groups n is generally equal to 3 but for ammonia in Hofmann clathrates, the four-fold symmetry of the host crystal induces an approximate 12-fold [44] or more complex [41, 45] symmetry. This tunneling is thus responsible for a rotation of the molecule forbidden in the classical case. The quantum rotobreather on an other hand is a state whose energy is situated *above* the energy of the separatrix. A tunneling effect appears, because of the coupling between molecules, which consists in the transfer of the excitation from site (molecule) to site. A study of the properties of the 4-

methyl-pyridine by Fillaux and co-workers has revealed the presence of a quantum sine-Gordon breather in this compound [3, 5, 17]. The properties of this state, shown to be the ground state of the system, are theoretically analyzed via a semiclassical quantization procedure of the classical solution of the sine-Gordon equation and then successfully compared to experimental results. However, the coupling between adjacent methyl groups is so strong along certain axes of the crystal (chains) that the relative phases on neighbouring groups are small. That allows to use the continuum sine-Gordon theory. In the case of a rotobreather, such an approximation becomes of course impossible due to the unavoidable large phase difference created at the interface between the rotating and oscillating groups. The study of the properties of rotobreathers (either classical or quantum) thus requires to preserve the rotational invariance of the interaction potential.

Our system under study consists of two pendula coupled by a cosine interaction potential (which preserves the rotational invariance). To simplify the study, the onsite and interaction potentials are the same functions and are 1-fold. This avoids to deal with the nearly degeneracies coming from the n different arches of a $\cos(nx)$ potential at low energies (typically below the separatrix). Notice that this does not change essentially the high energy part of the single site spectrum (which tends to the free rotor one whatever the value of n) but removes the splittings of the doublets which are not coming from the center ($k = 0$) or the edge ($k = n/2$) of the corresponding Brillouin zone $k \in \{-n/2+1, \dots, n/2\}$. The results we will obtain in section 2 concerning the upper part (above the separatrix energy) of the spectrum are thus easy to adapt to the case of an n -fold onsite potential. Notice at last that despite its very short size, our "pendula dimer" still possesses the discrete translational invariance \hat{T} which corresponds to the permutation symmetry.

The plan of the paper is as follows: in section 2 we briefly review the properties of a single quantum pendulum and we derive important formulas concerning the splitting occurring in the doublets in the high energy sector. In section 3, we start by presenting some results of the classical problem corresponding to two coupled pendula. Then we show how to compute the quantum spectrum of this system. We derive the exact spectrum at the uncoupled limit and we construct a quantum rotobreather according to the method presented in the introduction. By increasing the coupling between the pendula, we follow the quantum rotobreather (QR) and we compute the splittings occurring in the corresponding quadruplet.

II. SINGLE PENDULUM PROBLEM (SPP)

In this section we briefly review some of the properties of the classical and quantum one pendulum problem (for more details see for instance [46]). In the quantum case, we particularly focus on quasi-degenerated states

and their energy splitting. We show by two different methods that it is possible to compute this splitting exactly in leading order. The Hamiltonian of the pendulum system is given by

$$\mathcal{H}(x, p) = \frac{1}{2}p^2 + \alpha(1 - \cos(x)) \quad (1)$$

where x and p represent respectively the angle variable and the associated momentum. $\alpha > 0$ tunes the barrier height of the onsite potential.

A. Classical case

From (1) we deduce the classical equation of motion

$$\ddot{x} + \alpha \sin(x) = 0 \quad (2)$$

which possesses two different solutions. Denoting by E the energy of the pendulum and by $E_s = 2\alpha$ the energy of the separatrix separating the oscillatory motion from the rotational one we get:

- Oscillation: $E < E_s$

$$\sin(x/2) = k \operatorname{sn}(\sqrt{\alpha}t; k) \quad (3)$$

where the modulus of the Jacobian elliptic function sn is defined by the relation $k = (E/2\alpha)^{1/2}$ and the period of the oscillation is $T_{\text{osc}} = 4K(k)/\sqrt{\alpha}$, $K(k)$ being the complete elliptic integral of the first kind [47];

- Rotation: $E > E_s$

$$\sin(x/2) = \operatorname{sn}\left(\frac{\sqrt{\alpha}}{\tilde{k}}t; \tilde{k}\right) \quad (4)$$

where $\tilde{k} = (2\alpha/E)^{1/2}$ and where the rotation period is $T_{\text{rot}} = 2\tilde{k}K(\tilde{k})/\sqrt{\alpha}$.

B. Quantum case

Surprisingly, while the classical problem of the pendulum is a very basic one, it seems that a thorough study of the related quantum problem has been done quite recently (R. Aldrovandi and P. Leal Ferreira [46]). Our purpose here is not to repeat the analysis done in the paper cited above but rather to insist on the momentum reversal symmetry of the Hamiltonian (1) which leads to the appearance of pairs of quasi-degenerated states above the separatrix.

1. Analytical solution

The stationary Schrödinger equation corresponding to the Hamiltonian (1) is given by

$$-\frac{1}{2} \frac{d^2\psi(x)}{dx^2} + \alpha(1 - \cos(x))\psi(x) = E\psi(x). \quad (5)$$

ψ is the wave function of the pendulum and E its energy. As the wave function of the pendulum has to be single-valued ([46],[48]), we impose the periodicity condition

$$\psi(x + 2\pi) = \psi(x). \quad (6)$$

It is possible to get an analytical solution of (5) by performing the following change of variables: $u = (\pi - x)/2$ and $\phi(u) = \psi(x)$. We immediately obtain the canonical form of the Mathieu equation ([47])

$$\frac{d^2\phi(u)}{du^2} + (a - 2q \cos(2u))\phi(u) = 0 \quad (7)$$

where

$$q = 4\alpha \quad \text{and} \quad a = 8(E - \alpha). \quad (8)$$

Because of the previous change of variables, $\phi(u)$ is now a π -periodic function. It can be shown ([47]) that the Mathieu equation supports π -periodic solutions if and only if the characteristic value a belongs to an infinite countable set of values denoted by $\{a_{2n}(q), b_{2n}(q)\}$ $n \in \mathbb{N}$. a_{2n} is related to the *even* Mathieu function $ce_{2n}(u, q)$ whereas b_{2n} is related to the *odd* Mathieu function $se_{2n}(u, q)$. As follows from their definition (8), q is directly related to the energy of the separatrix $E_s = 2\alpha$ that is to the depth of the cosine potential appearing in the Schrödinger equation whereas, up to a scaling and a shift factor, a represents the eigenenergies of the pendulum Hamiltonian. For a given value of q (that is of α), the series $\{a_{2n}, b_{2n}\}$ increases monotonically with n keeping the property $b_{2n} < a_{2n}$. For $n = 0$ the only possible solution is an even function $ce_0(u, q)$ which represents the ground state of the system.

According to the previous results, the analytical solution of the Schrödinger equation (5) reads

$$\begin{aligned} \psi_{2n}^{(e)} &= \frac{1}{\sqrt{\pi}} ce_{2n}\left(\frac{\pi - x}{2}, q\right) ; & E_{2n}^{(e)} &= \frac{a_{2n}(q)}{8} + \alpha \\ \psi_{2n}^{(o)} &= \frac{1}{\sqrt{\pi}} se_{2n}\left(\frac{\pi - x}{2}, q\right) ; & E_{2n}^{(o)} &= \frac{b_{2n}(q)}{8} + \alpha \end{aligned} \quad (9)$$

for $n \in \mathbb{N}^*$ and

$$\psi_0^{(e)} = \frac{1}{\sqrt{\pi}} ce_0\left(\frac{\pi - x}{2}, q\right) ; \quad E_0^{(e)} = \frac{a_0(q)}{8} + \alpha \quad (10)$$

for $n = 0$ which represents the ground state of the pendulum Hamiltonian.

2. The Fourier representation (FR)

According to the periodicity condition (6) imposed to the wave function, it is rather natural to consider its Fourier expansion:

$$\psi(x) = \frac{1}{\sqrt{2\pi}} \sum_{m \in \mathbb{Z}} \psi_m e^{imx} \quad (11)$$

where

$$\psi_m = \frac{1}{\sqrt{2\pi}} \int_0^{2\pi} \psi(x) e^{-imx} dx. \quad (12)$$

Because of the periodicity of the wave function, the Fourier space associated to the pendulum problem is infinite but discrete. In the FR, the stationary Schrödinger equation becomes

$$m^2 \psi_m - \alpha(\psi_{m+1} + \psi_{m-1}) = \tilde{E} \psi_m \quad , \quad m \in \mathbb{Z} \quad (13)$$

where for later convenience we have redefined the energy as

$$\tilde{E} = 2(E - \alpha). \quad (14)$$

Equation (13) represents a tight-binding equation whose hopping terms and onsite potential would be respectively $-\alpha$ and m^2 . In this equation, the sum $(\psi_{m+1} + \psi_{m-1})$ related to the cosine potential plays now the role of a discrete Laplacian while the onsite "potential" term m^2 comes from the kinetic energy. Thus, in FR, the terms of the Schrödinger equation have inverted their role. This fact is important in understanding how the Discrete Wentzel-Kramers-Brillouin (DWKB) method ([49],[50]) applies to the Mathieu equation (see section IIB 6).

Equation (13) is invariant under the transformation $(m \rightarrow -m)$. This symmetry operation corresponds to the inversion of the momentum of the system ($p \rightarrow -p$) which originates in the time reversal symmetry of the original problem. This allows us to separate the eigenstates of (13) into symmetric $|s\rangle$ and antisymmetric $|a\rangle$ states.

We may write the Hamiltonian of (13) as

$$\tilde{H} = \sum_{m \in \mathbb{Z}} m^2 |m\rangle \langle m| - \alpha(|m+1\rangle \langle m| + |m\rangle \langle m+1|) \quad (15)$$

where we have used the ket notation $|m\rangle$ to represent the plane wave function $\langle x|m\rangle = e^{imx}/\sqrt{2\pi}$. The matrix representing \tilde{H} in the FR is infinite, tridiagonal and symmetric. Its diagonal elements are m^2 and the off-diagonal elements are constant and equal to $-\alpha$. Moreover, $\tilde{H}_{m,n} = \tilde{H}_{-m,-n}$. This additional "central" symmetry is a direct consequence of the time reversal symmetry and the Hermitian properties of \tilde{H} .

3. Low-energy states

Without any onsite potential ($\alpha = 0$), it follows from (15) that $|m\rangle$ and $|-m\rangle$ are eigenstates of \tilde{H} with identical energy m^2 . Consequently, each state except the ground state $|0\rangle$ is two-fold degenerated in this limit. This two-fold degeneracy is due to the two equivalent possible motions consisting in rotating in a given sense or its opposite.

The switching on of an onsite potential governed by the parameter α lifts this degeneracy but in a way depending on the energy level of the state under consideration. Indeed, when α becomes nonzero, the pendulum system admits a new kind of motion, namely, the oscillating motion which corresponds to the motion in the cosine arch of the potential well in the classical system (see Fig. 1). The quantum system also admits such kind of states but their number is limited by the value of α because of the quantization rules. As α becomes larger, the number of states below the separatrix increases and can be estimated to $8\sqrt{\alpha}/\pi$ by using the Weyl formula (see below (27) in the limit $k \rightarrow 1$). If the value of α is large enough it becomes possible to look at the properties of the low energy states by expanding the cosine potential around zero in a series of powers of x . We obtain

$$\alpha(1 - \cos(x)) = \alpha \left(\frac{1}{2}x^2 - \frac{1}{24}x^4 + \frac{1}{720}x^6 + \circ(x^7) \right). \quad (16)$$

The first order of this expansion leads to the harmonic approximation of (1) whose frequency is given by $\omega = \sqrt{\alpha}$. Thus, low energy states of the quantum pendulum are well represented by the corresponding low energy harmonic eigenstates (at least for large enough values of α). As the level spacing of the harmonic oscillator is constant (and equal to ω) we expect the states to be quite regularly spaced deep inside the well. This is illustrated in Fig. 1 which represents the lower part of the spectrum of a pendulum whose parameter $\alpha = 50$. The energy levels of $|s\rangle$ and $|a\rangle$ states have been respectively represented to the right and to the left. We clearly see that the few first states are quite regularly spaced while they condensate in reaching energies close to the separatrix. By using standard second order perturbation theory within the natural harmonic basis, we may obtain the first corrections to the pure harmonic spectrum. This perturbation in the nonlinear terms gives

$$E_n = \frac{1}{2}(n + (n+1))\omega - \frac{1}{2^5}(n^2 + (n+1)^2) - \frac{1}{2^9}(n^3 + (n+1)^3)\frac{1}{\omega} + \mathcal{O}\left(\frac{1}{\omega^2}\right) \quad (17)$$

where n labels the states ($n \in \mathbb{N}$). Of course, this expression ceases to be valid when nonlinear corrections become large as compared to the harmonic term. Nevertheless, it shows how the spacing becomes smaller as the energy increases but remains below the energy of the separatrix:

$$\Delta_n = E_{n+1} - E_n \simeq \left(\omega - \frac{1}{8} - \frac{1}{64\omega} \right) - \left(\frac{1}{8} + \frac{3}{128\omega} \right) n - \frac{3}{256\omega} n^2. \quad (18)$$

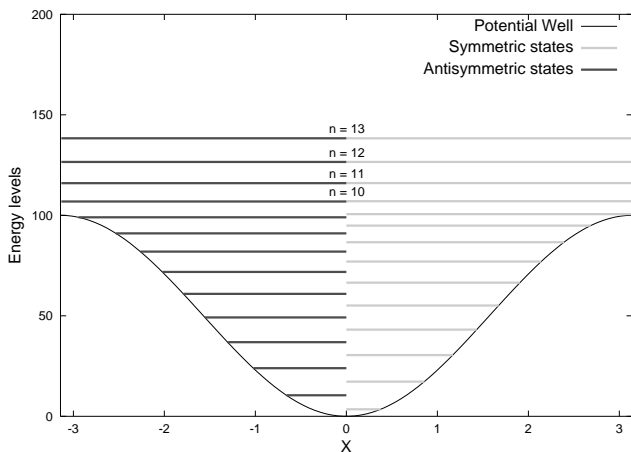


FIG. 1: Energy levels of a pendulum with $\alpha = 50$. States have been distinguished according to their parity. Only a few states lying above the separatrix have been displayed. The number n of the corresponding doublet is written on top of it.

4. High-energy states

Above the separatrix, Fig. 1 shows that symmetric and antisymmetric states glue together to form pairs of nearly degenerated states. From a physical point of view this phenomenon is due to the fact that far above from the separatrix the cosine potential appears like a perturbation of the free rotor and only shifts the levels a bit around their value $\tilde{E}_m^{\text{free rotor}} = m^2$ ($m^2 \gg 2\alpha$). Because of the momentum reversal symmetry, the Hamiltonian (15) diagonalizes into two blocks each related respectively to $|s\rangle$ or $|a\rangle$ states. In the FR, the corresponding reduced matrices are still tridiagonal. By applying standard perturbation theory in the parameter α to one of these matrices whose spectrum is now free of nearly degenerated eigenvalues, we obtain corrections to the free rotor energy $\tilde{E}_m^{\text{free rotor}} = m^2$. To second order, we find

$$\tilde{E}_n^d = n^2 + \frac{2\alpha^2}{4n^2 - 1} + \mathcal{O}\left(\frac{\alpha^4}{n^6}\right). \quad (19)$$

Explicit corrections up to α^6/n^{10} are obtainable (see [47] p. 724). As we mentioned, this energy is the mean energy of a doublet. This is indicated by the subscript d in (19).

5. Analytical computation of the splitting: High-order perturbation theory

It is also possible to calculate explicitly the splitting between the symmetric and antisymmetric states of a doublet labeled by m ($m^2 \gg 2\alpha$). The inverse of this splitting is a direct measure of the time required by a rotating state to invert its initial momentum. It has to be noticed that by "rotating state" we mean the superposition of the states $|s\rangle$ and $|a\rangle$ belonging to the same dou-

blet. Because of their symmetry, the expectation value of the momentum for $|s\rangle$ and $|a\rangle$ are zero.

A possible way to get this splitting is to use high order perturbation theory as it has already been done in [12] (equation (12)). A proof of this formula has been derived in [4] and applied to the quantum discrete self-trapping equation. The special "centro-symmetric" form of the tridiagonal Hamiltonian matrix in the FR allows us to compute the exact leading order of the splitting as

$$\Delta E_n = \frac{1}{2} \Delta \tilde{E}_n = \frac{1}{8} (a_{2n}(4\alpha) - b_{2n}(4\alpha)) = \frac{\alpha^{2n}}{(2n-1)!^2}. \quad (20)$$

Notice that due to the obvious relation between the eigenfunctions of the SPP and the Mathieu functions, the splitting ΔE_n gives in turn the result of the splitting between the characteristic values associated to the symmetric and antisymmetric π -periodic Mathieu functions ce_{2n} and se_{2n} . A similar computation allows us to obtain the splitting for the 2π -periodic Mathieu functions. By using the notations of [47], we get

$$a_r(q) - b_r(q) = \frac{8}{(r-1)!^2} \left(\frac{q}{4}\right)^r + o(q^{r+1}) \quad \text{as } r \rightarrow \infty. \quad (21)$$

To our knowledge this is the first time that such a splitting has been exactly computed in leading order [68]. In particular, it corrects and precises the formula obtained in [47]. Moreover, it can be verified to be correct by using the small q expansions of the low order characteristic values themselves.

As n , which represents the label of the doublet, becomes large enough, we find the following asymptotic form for the splitting

$$\Delta E_n \sim \left(\frac{n}{\pi} - \frac{1}{12\pi}\right) \left(\frac{e\sqrt{\alpha}}{2n}\right)^{4n} \quad (n \rightarrow \infty) \quad (22)$$

indicating that it decays more than exponentially fast as n increases. Moreover this expression contains its limit of validity as the number n has to be greater than the critical value $n_c = e\sqrt{\alpha}/2$ to ensure that the splitting is small (see comment [69]).

6. Discrete WKB theory

Another way to compute the doublet splitting is to use the DWKB method developed in [49] and to use the discrete counterpart of the Herring's formula as done in [50]. Following [50] and according to (13), the splitting between the nearly degenerated states reads

$$\Delta E_n = \frac{1}{2} |\tilde{E}_s^{(n)} - \tilde{E}_a^{(n)}| = \alpha s_0^{(n)} a_1^{(n)} \quad (23)$$

where $s_0^{(n)}$ and $a_1^{(n)}$ are the Fourier components of the symmetric and antisymmetric states of the n -th doublet.

Instead of evaluating these components by using the connection formulae of [49], we use directly the resulting forms given in [47]. The asymptotic behavior (see expression 20.2.29 of [47]) of the Fourier components of the Mathieu functions yields

$$A_0^{(2n)}(q) = \frac{(n-1)!}{n!(2n-1)!} \frac{q^n}{4^n} A_{2n}^{2n}(q)$$

$$B_2^{(2n)}(q) = \frac{n!}{(n-1)!(2n-1)!} \frac{q^{n-1}}{4^{n-1}} B_{2n}^{2n}(q)$$

where A and B are the coefficients of the cosine and sine Fourier series of the π -periodic Mathieu functions ce_{2n} and se_{2n} . The superscript indicates the order whereas the subscript labels the Fourier components. The correct normalization yields $s_0^{(n)} = \sqrt{2}A_0^{(2n)}(q)$ and $a_1^{(n)} = B_2^{(2n)}(q)/\sqrt{2}$ (see (9) and (11)). By taking into account that $A_{2n}^{2n}(q) = B_{2n}^{2n}(q) = 1 + o(q)$ and $\alpha = q/4$, we finally get

$$\Delta E_n = \frac{\alpha^{2n}}{[(2n-1)!]^2} \quad (24)$$

which coincides with (20). The graph (Fig. 2) shows the spacings and the splittings of the SPP spectrum for $\alpha = 50$ as a function of the energy E . The crosses correspond to $E_{n+1} - E_n$ as obtained from the numerical diagonalization of (13). The two upper branches (dotted line) represent the spacing between *neighboring eigenvalues* (when $E < E_s$) and the spacing between the *doublets* (when $E > E_s$) computed by using the density of states (26). They are shown to be in excellent agreement with the numerical data. The splitting, that is, the energy difference between the states $|s\rangle$ and $|a\rangle$ of the doublets is represented by the third branch which is decreasing rapidly as the energy increases. Again, the analytical result (solid curve) given by (24) is excellent. The inset shows a comparison between this analytical splitting and the numerical result of the numerical splitting obtained by using Herring's formula (23). Notice that the splitting can be now as small as 10^{-120} although it has been computed with a simple FORTRAN scheme in double precision (16 digits). Because the eigenvalues are of order of unity it is of course impossible to obtain such a result by subtracting two neighboring eigenvalues obtained by diagonalizing (13) in double precision. The precision is in this case limited to $\sim 10^{-14}$. But the way to compute the eigenvectors makes it possible inasmuch as the numerical limit becomes not the number of digits but the smallest number representable by the computer. This result shows that it is possible to compute very small splittings by using common FORTRAN routines instead of using high precision schemes provided by Mathematica or MAPLE for instance.

An equally important property of the DWKB method is that it provides with a simple and nice picture of the basic properties of the eigenstates. Indeed, as explained in [49], it is possible to associate a "classical" Hamiltonian defined by $H_{cl} = m^2 - 2\alpha \cos \phi$ to the three-term

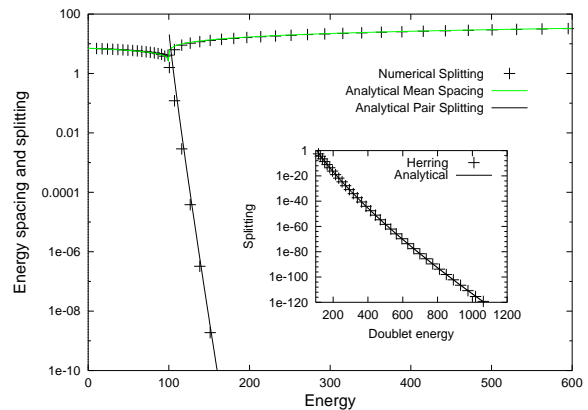


FIG. 2: Spacings and splittings of the spectrum of a quantum pendulum for $\alpha = 50$. Quantities are described in the text.

recursion relation (13), where m and ϕ correspond to the conjugated "coordinate" and "momentum". This definition is rather natural as $\hat{\phi} \equiv -i\partial/\partial m$ is precisely the Fourier representation of the angular variable x . Interpreting ϕ as a momentum, the expression of H_{cl} shows that its classical motion is confined between two "potential" curves defined by $U^\pm(m) = m^2 \pm 2\alpha$ (see Fig. (3)). The idea is then to use this fact to compute the DWKB solution related to this "classical" Hamiltonian. The internal region defined by the two parabolas $U^\pm(m)$ represents the classical allowed region whereas the regions outside are forbidden. The eigenfunctions are thus localized on the allowed region while they decay exponentially (or faster) in the forbidden ones. This provides a natural way to express their location and their extension on the Fourier lattice according to their energy. We find indeed that at sufficiently high energy (far above the separatrix) the eigenfunction of energy $E \sim m^2/2 + \alpha$ is localized around m and $-m$ whatever its parity. Its localization length around these two centers is roughly given by $L(E) = \sqrt{\tilde{E} + 2\alpha} - \sqrt{\tilde{E} - 2\alpha} \sim E_s/\sqrt{2(E - \alpha)}$ as $E \gg E_s = 2\alpha$. The localization length in the Fourier space thus decreases like the square root of the energy.

7. Density and number of states

We end this section devoted to the properties of the single pendulum problem by giving the expressions of the number $n(E)$ and the density $\rho(E)$ of states computed by the mean of Weyl formula:

$$\rho(E) = \frac{1}{2\pi} \int \delta(E - H(x, p)) dx dp. \quad (25)$$

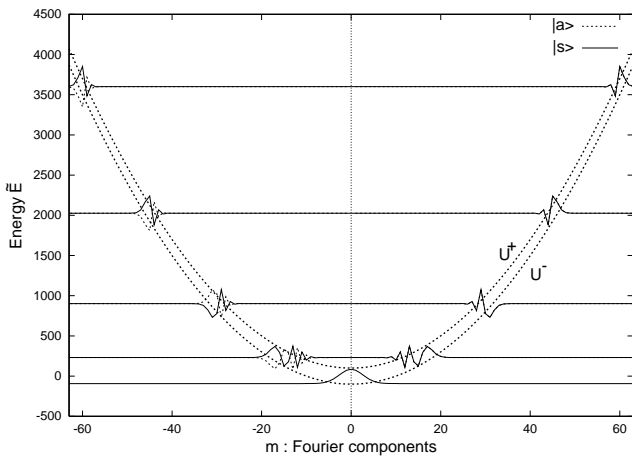


FIG. 3: "Potential" curves U^\pm used in the DWKB theory to compute the eigenfunctions of the SPP. Some symmetric (solid) and antisymmetric (dashed) eigenfunctions have been superposed to them. Their base line situated at their energy level allows to compare the location and the width of their peaks to the interval between the potential curves U^\pm . The value of α is 50. For the sake of visibility, the wave functions have been multiplied by a suitable scaling factor.

It yields

$$\begin{aligned} \rho(E) &= \frac{2\sqrt{2}}{\pi\sqrt{E}} k\mathcal{K}(k) \quad , \quad E < 2\alpha ; \quad k = \sqrt{\frac{E}{2\alpha}} \\ &= \frac{2\sqrt{2}}{\pi\sqrt{E}} \mathcal{K}(k) \quad , \quad E > 2\alpha ; \quad k = \sqrt{\frac{2\alpha}{E}} \end{aligned} \quad (26)$$

and by integrating

$$\begin{aligned} n(E) &= \frac{8\sqrt{\alpha}}{\pi} (\mathcal{E}(k) - k'^2\mathcal{K}(k)) \quad , \quad E \leq 2\alpha \\ &= \frac{4\sqrt{2E}}{\pi} \mathcal{E}(k) \quad , \quad E \geq 2\alpha \end{aligned} \quad (27)$$

with the same definition of k than above. In these expressions $\mathcal{E}(k)$ and $\mathcal{K}(k)$ denote the usual complete elliptic integrals of the first and second kind (see e.g. [47]). The above expressions of $\rho(E)$ show that the density of states develops a logarithmic divergency close to the separatrix. In this limit, its expression reads $\rho(E) \sim \ln(16E/|E - E_s|)/(\pi\sqrt{\alpha})$. This phenomenon is known as a Van Hove singularity [51] and has also been discussed for the case of the quantum dimer [12]. The graph (Fig. 4) shows the excellent agreement between the density of states (DOS) computed by the mean of Weyl's formula and the DOS computed numerically by diagonalization of (13).

Using (27), we may now obtain the splitting ΔE as a function of the doublet energy E :

$$\Delta E(E) \approx \frac{\alpha \frac{4\sqrt{2E}}{\pi} \mathcal{E}\left(\sqrt{\frac{2\alpha}{E}}\right)}{\left[\Gamma\left(\frac{4\sqrt{2E}}{\pi} \mathcal{E}\left(\sqrt{\frac{2\alpha}{E}}\right)\right)\right]^2} \quad (E \rightarrow \infty). \quad (28)$$

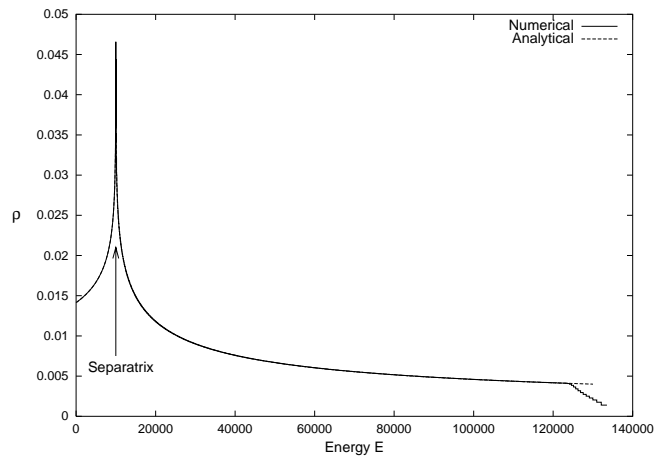


FIG. 4: Density of states for a pendulum with parameter $\alpha = 5 \cdot 10^3$. Numerical data have been obtained from (15) for a matrix truncated to 1001 Fourier components ($-500 \leq m \leq 500$). Comparison with analytical expression (26) shows an excellent agreement until truncation errors become important ($E \sim 1.25 \cdot 10^5$).

III. TWO COUPLED PENDULA

The Hamiltonian of the two coupled pendula is given by

$$\begin{aligned} H &= H_1 + H_2 + H_{\text{int}} \\ &= \sum_{i=1}^2 \left\{ \frac{p_i^2}{2} + \alpha(1 - \cos x_i) \right\} + \varepsilon(1 - \cos(x_1 - x_2)) \end{aligned} \quad (29)$$

where $\varepsilon > 0$ represents the coupling parameter between the pendula.

The coupling has been chosen to be periodic in $(x_1 - x_2)$ to allow solutions where one pendulum is oscillating whereas the other one is rotating. This condition is of course essential to obtain rotobreather type solutions. Notice finally that such a Hamiltonian has already been used to describe classical nonlinear rotating modes in a chain of coupled pendula [52].

The Hamiltonian (29) possesses two different symmetries. One is related to the exchange of the coordinates of the two pendula $\{\mathcal{S}_p : (x_1, p_1) \leftrightarrow (x_2, p_2)\}$ and the other to the reversal of the global momentum of the system, $\{\mathcal{S}_m : (p_1 + p_2) \leftrightarrow -(p_1 + p_2)\}$. The latter represents the generalization of the momentum reversal symmetry already observed in the single pendulum system.

A. Classical rotobreather

Although the system is invariant with respect to the permutation of the coordinates, some solutions of the equations of motion are not. Indeed, there exist exact solutions of the Hamilton equations derived from (29),

which consist of two pendula oscillating at the same frequency but with different amplitudes. It is also possible to obtain solutions where one pendulum is oscillating whereas the other one is rotating, both again evolving at the same frequency. Hereafter, both kinds of solutions will be respectively referred to as "breather" and "rotobreather" solutions. Of course, because of the size of our system, the exponential spatial decay property of usual breathers becomes meaningless and the classical breather type solution refers only to exact time-periodic solutions which break the permutation symmetry \mathcal{S}_p .

As Poincaré sections (PS) are known to be a useful tool in describing the behavior of non integrable dynamical systems, we will use them to locate the orbits of the classical rotobreathers at a given energy. This energy has to be larger than the separatrix level of the SPP to allow one of the pendula to rotate whereas the other one is at rest in the uncoupled (anti-continuous) limit ($\varepsilon = 0$). But this energy can not be too close to the SPP separatrix as ε becomes non zero. Indeed, the system develops a chaotic layer in its vicinity and prevents any stable periodic solution of the rotobreather type from existing. Concerning the classical rotobreather itself it is obtained by using standard numerical methods like a Newton scheme or a variational method (see e.g. [15],[29]). The purpose of this paper is not to carry out an extensive study of the classical system but merely to deal with its quantum counterpart. Consequently we will just give here an example of a classical rotobreather. The values of the parameters are $\alpha = 5$, $\varepsilon = 1$. The energy of the rotobreather is $E_b \simeq 31.77$ and its period $T_b \simeq 0.885$. The initial data are $p_1^b \simeq 7.969$, $p_2^b \simeq -0.160$, $x_1^b = 0$ and $x_2^b = -5.2 \cdot 10^{-9}$. The first pendulum is rotating whereas the second one is librating. The graph Fig.5 represents two Poincaré sections realized with the condition $x_1 = 0$ at an energy fixed to E_b . The first PS is plotted in the phase space of the second pendulum. As its trajectory is strictly periodic, the Poincaré section of the rotobreather orbit simply consists of a single point. It has been represented by a "star" symbol. Other periodic trajectories present in this system have been represented by a "cross" and a "times". They respectively show the in-phase and out-of-phase motions which are symmetric modes and thus can not be considered as breathers. The second PS represents the same situation in the momenta space. Given the natural Fourier representation of the quantum problem due to the 2π -periodicity of the wave function, it provides the ideal frame for the comparison of the classical and the quantum situations. Notice that because of the existence of symmetries the presented rotobreather solution is not the only one. Indeed, in the momentum space (p_1, p_2) , the global momentum reversal symmetry is nothing but the reflection symmetry with respect to the point $(p_1 = 0, p_2 = 0)$. And the permutation symmetry is the mirror symmetry with respect to the line $p_1 = p_2$. Using these two symmetries we easily obtain the location of the four classical rotobreather solutions $(\pm p_1^b, \pm p_2^b)$. Nevertheless, and despite these symmetries,

if the system starts initially on one of the classical rotobreather orbits, it remains on this orbit for an infinite time. This prevents the classical system from transferring the initial excitation from one pendulum to the other. We will see that such a situation is impossible to be realized in the quantum system.

In order to find the quantum counterpart of the classical rotobreather, we will proceed exactly as in the classical case. Starting from the anti-continuous limit where we know the classical rotobreather to exist, we will find the corresponding quantum state and study its evolution with respect to the coupling ε .

B. 2D Fourier space

The state of the two pendula system $\psi(x_1, x_2)$ has to be 2π -periodic in each of its variables as in the single pendulum problem. We thus expand it as a double Fourier series

$$|\psi\rangle = \sum_{(m,n) \in \mathbb{Z}^2} \psi_{m,n} |m,n\rangle \quad (30)$$

where $|m,n\rangle = |m\rangle \otimes |n\rangle$ and $\langle x|n\rangle = \exp(inx)/\sqrt{2\pi}$. With (29), the eigenvalue equation $H|\psi\rangle = E|\psi\rangle$ reads

$$\begin{aligned} \tilde{E}\psi_{m,n} &= (m^2 + n^2)\psi_{m,n} - \alpha(\psi_{m+1,n} + \psi_{m-1,n}) \\ &\quad - \alpha(\psi_{m,n+1} + \psi_{m,n-1}) - \varepsilon(\psi_{m+1,n-1} + \psi_{m-1,n+1}) \end{aligned} \quad (31)$$

where $\tilde{E} = 2(E - 2\alpha - \varepsilon)$ is a shifted and rescaled energy. In this discrete Fourier space, the symmetry operations \mathcal{S}_m and \mathcal{S}_p become: $\{\mathcal{S}_m|(m,n) \rightarrow (-m,-n)\}$ (momentum reversal) and $\{\mathcal{S}_p|(m,n) \rightarrow (n,m)\}$ (permutation). As H is invariant under these symmetries, it commutes with the corresponding operators and its eigenstates gather naturally in four different symmetry classes. We denote the four different kinds of eigenstates by $\{|s\rangle, |a\rangle, |\bar{s}\rangle, |\bar{a}\rangle\}$. Their symmetry properties are listed hereafter.

State	Momentum reversal \mathcal{S}_m	Permutation \mathcal{S}_p
$ s\rangle$	$S \quad s_{m,n} = s_{-m,-n}$	$S \quad s_{m,n} = s_{n,m}$
$ a\rangle$	$A \quad a_{m,n} = -a_{-m,-n}$	$S \quad a_{m,n} = a_{n,m}$
$ \bar{s}\rangle$	$S \quad \bar{s}_{m,n} = \bar{s}_{-m,-n}$	$A \quad \bar{s}_{m,n} = -\bar{s}_{n,m}$
$ \bar{a}\rangle$	$A \quad \bar{a}_{m,n} = -\bar{a}_{-m,-n}$	$A \quad \bar{a}_{m,n} = -\bar{a}_{n,m}$

S and A indicate respectively that the state is symmetric or antisymmetric with respect to the corresponding symmetry. To evaluate numerically the eigenvalues and eigenvectors of (31), we truncate the (normally infinite) system to $-N \leq m, n \leq N$, where N is chosen sufficiently large to prevent any important truncation errors for states whose energy $\tilde{E} \ll 2N^2$. In this case, the total number of computed eigenvalues is $(2N+1)^2$. Due to the symmetries, we only diagonalize the sub-matrices representing the four different classes of eigenvectors. The rank of the sub-matrices related to $|s\rangle, |a\rangle, |\bar{s}\rangle$ is $(N+1)^2$, $N(N+1)$, $N(N+1)$ and N^2 respectively.

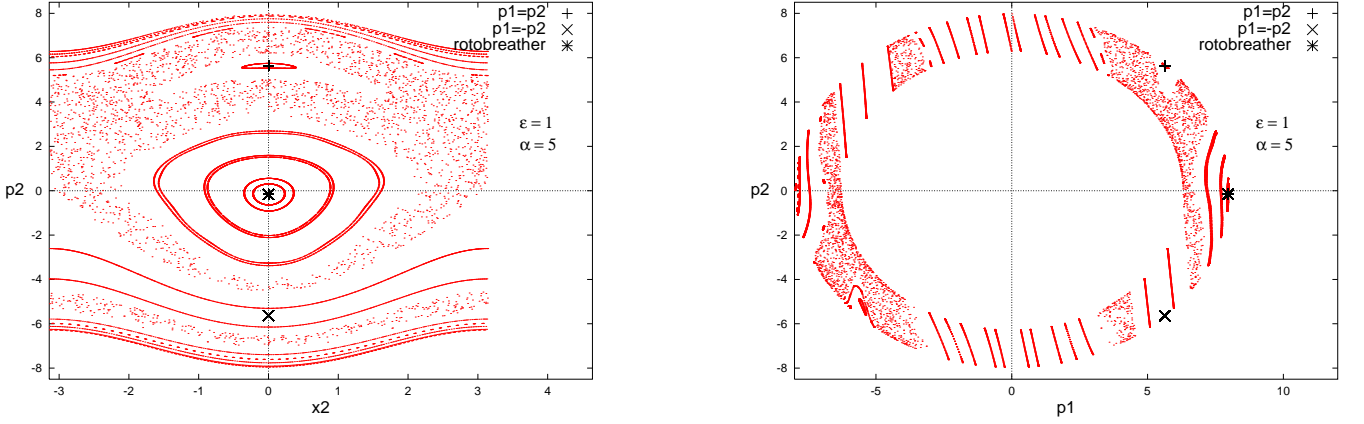


FIG. 5: Poincaré sections of the two coupled pendula system in the phase space of the second pendulum (left) and in the momenta space (right). The conditions of the maps are $x_1 = 0, p_1 > 0$ (left) and $x_1 = 0, x_2 > 0$ (right). The energy $E = 31.77$. In-phase (cross), out-of-phase (times) and rotobreather (star) trajectories are represented.

C. The global spectrum at the anti-continuous limit ($\varepsilon = 0$)

There are two limiting cases where the eigenvalue equation (31) can be solved analytically. These correspond to situations where the classical system becomes integrable. The first one is realized when the coupling parameter ε is equal to zero, i.e. where the system consists of two identical decoupled pendula. The second one is realized when the onsite parameter α becomes zero, where, by passing to the center-of-mass representation, the system can be reduced to a free rotor plus a decoupled pendulum. In these two limits the global spectrum of the system is given by the sum of two one-particle spectra. Moreover, in the limit where ε is equal to zero, the two spectra are identical. This leads to a two-fold degeneracy of the main part of the global spectrum. Nevertheless, by constructing the eigenvectors in such a way that they belong to a given symmetry class, the eigenstates are unambiguously defined and already represent the proper zeroth order states suitable for any perturbation calculation in ε .

1. Limit of zero onsite parameter: ($\alpha = 0$)

Let us first derive some results concerning the anti-continuous limit ($\varepsilon = 0$) when the onsite parameter is itself equal to zero ($\alpha = 0$). In this case, the system consists of two free rotors and the global spectrum is straightforwardly given by

$$\tilde{E}_{m,n} = m^2 + n^2. \quad (32)$$

The corresponding eigenstates are given by a product of correctly symmetrized plane waves. Namely,

$$\begin{aligned} |s\rangle &= \frac{1}{2} (|m, n\rangle + |-m, -n\rangle + |n, m\rangle + |-n, -m\rangle) \\ |a\rangle &= \frac{1}{2} (|m, n\rangle - |-m, -n\rangle + |n, m\rangle - |-n, -m\rangle) \\ |\bar{s}\rangle &= \frac{1}{2} (|m, n\rangle + |-m, -n\rangle - |n, m\rangle - |-n, -m\rangle) \\ |\bar{a}\rangle &= \frac{1}{2} (|m, n\rangle - |-m, -n\rangle - |n, m\rangle + |-n, -m\rangle). \end{aligned}$$

Notice that $\tilde{E}_{m,n}$ is a nonnegative integer in this limit. Its degeneracy can be expressed as follows (result due to Gauss, see e.g. [53]):

Let $\tilde{E} \in \mathbb{N}^*$ and

$$g(\tilde{E}) = \#\{(m, n) \in \mathbb{Z}^2 : m^2 + n^2 = \tilde{E}\}$$

be the degeneracy of the level \tilde{E} . Let

$$\tilde{E} = \prod_{\text{prime } p} p^{e(p)}$$

be its prime number factorization. If $\forall p \equiv 3 \pmod{4}, e(p) \equiv 0 \pmod{2}$, then \tilde{E} can be written as the sum of two squares, i.e. $g(\tilde{E}) \neq 0$ (Fermat). In this case (Gauss), its degeneracy is given by

$$g(\tilde{E}) = 4 \prod_{p \equiv 1 \pmod{4}} (e(p) + 1). \quad (33)$$

Moreover, the number of states (i.e. the integrated density of states) behaves asymptotically as

$$n(\tilde{E}) = \sum_{\tilde{E}' \leq \tilde{E}} g(\tilde{E}') = \pi \tilde{E} + \mathcal{O}(\sqrt{\tilde{E}}) \quad (\tilde{E} \rightarrow \infty). \quad (34)$$

2. Switching on the onsite potential ($\alpha \neq 0$)

The last expression is not only valid in the limit of free rotors but also when α and ε are non zero. This is confirmed by the Weyl's formula which indicates the zeroth order term of the degeneracy $g(\tilde{E})$. Indeed ([54] p.497, 21.4)

$$g_{\text{Weyl}}(\tilde{E}) = \frac{1}{2} \left(\frac{1}{2\pi} \int_{\tilde{V}(x_1, x_2) < \tilde{E}} dx_1 dx_2 \right) \quad (35)$$

where $-\tilde{V}(x_1, x_2)/2 = \alpha(\cos x_1 + \cos x_2) + \varepsilon \cos(x_1 - x_2)$. The prefactor $1/2$ is coming from the rescaling of \tilde{E} as compared to E . As $(x_1, x_2) \in]-\pi, \pi]^2$, when $\tilde{E} > \tilde{E}^+ = \max(\tilde{V}(x_1, x_2))$, the integral term is constant and equal to $(2\pi)^2$. Thus $g_{\text{Weyl}}(\tilde{E}) = \pi$ and $n_{\text{Weyl}}(\tilde{E}) = \pi\tilde{E} + \text{const}$ when $\tilde{E} > \tilde{E}^+$. It is possible to show by direct calculation that the constant term is equal to zero and that $\tilde{E}^+ = 2(2\alpha - \varepsilon)$ if $\alpha \geq 2\varepsilon$ or $\tilde{E}^+ = 2(\varepsilon + \alpha^2/2\varepsilon)$ if $\alpha \leq 2\varepsilon$. As \tilde{E}^+ gives the "top" of the potential for any values of the parameters ε and α , it also represents a natural transition value in the global spectrum indicating the level at which the influence of the potential V starts to be weak.

Expression (34) thus provides a very useful guide for checking the energy level at which truncation errors become important. Note that truncation errors are of two types. First, because of the truncation of the whole matrix, there exists an energy threshold for which some eigenvalues of the spectrum are missing. Indeed for $\varepsilon = 0$, the global spectrum is given by the sum of the SPP spectrum with itself. In this case, even assuming that the numerically computed eigenvalues are exact, the SPP spectrum ends at \tilde{E}_e^{SPP} because of truncation. Let us denote the energy of its ground state by \tilde{E}_0^{SPP} . Then the first eigenvalue to be missed is $\tilde{E}_{e+1}^{\text{SPP}} + \tilde{E}_0^{\text{SPP}}$ where $\tilde{E}_{e+1}^{\text{SPP}}$ is the first eigenvalue following \tilde{E}_e^{SPP} . This provides with a threshold where the eigenvalues start to be ranked in a wrong way. Their label becomes false and so does the computed number of states $n(\tilde{E})$. This is shown in Fig. 6 which represents the spectrum of two uncoupled pendula as computed from equation (31) for different values of N (recall that $-N \leq m, n \leq N$). The second type of error induced by the truncation is a modification of the values of the energies themselves. As we have verified these errors increase as we reach the upper end of the truncated spectrum but are nevertheless very small if we respect the threshold indicated above.

Although the degeneracy (33) has been obtained for the case where both the onsite and the coupling parameters are zero, it provides with useful information when considering the near degeneracy of n -uplets arising at sufficiently high energy (that is, far above twice the energy of the separatrix of the SPP).

As the onsite parameter α becomes different from zero, the first part of the free rotor spectrum of the SPP is modified. Far below the SPP's separatrix, the quadratic spectrum $\tilde{E}_l^{\text{SPP}} = l^2$ is replaced by a harmonic oscillator

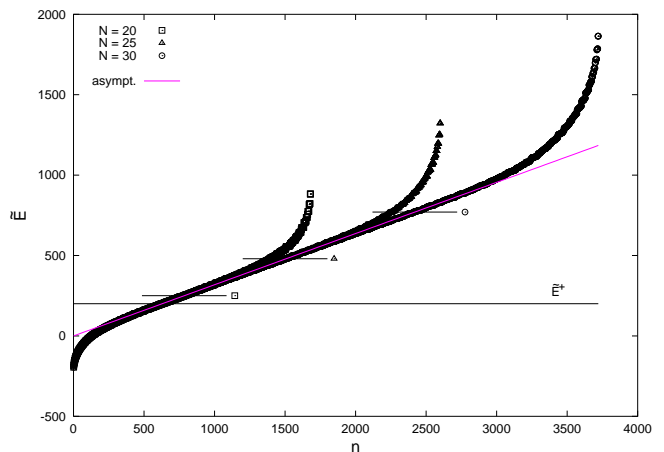


FIG. 6: Spectrum of the global uncoupled ($\varepsilon = 0$) system computed by diagonalizing (31) for different values of the maximal number of Fourier components N of the wave function $|\psi\rangle$. The linear dimension of the Hamiltonian matrix is $(2N + 1)^2$. $\alpha = 50$. \tilde{E}^+ (see text) has been indicated as well as the thresholds where, because of truncation, the computed spectrum starts to be larger gapped. Thresholds are represented by straight lines ended by the symbol of the corresponding spectrum. The asymptote $\tilde{E} = n/\pi$ is also shown.

one $\tilde{E}_l^{\text{SPP}} \sim 2(\sqrt{\alpha}l - \alpha)$. The number of states $n(\tilde{E})$ of the global uncoupled system thus becomes a quadratic function of the energy. This explains the form of the function $\tilde{E}(n)$ observed in Fig.6 which starts as a square root and asymptotically becomes a linear function of n .

D. Quantum rotobreather state

1. Anti-continuous limit

The goal of this paper is to define and to study a quantum rotobreather state $|\Phi\rangle$ whose properties are very similar to those of the classical rotobreather. Consequently it is natural to look for a quantum state which, at the anti-continuous limit ($\varepsilon = 0$), represents a state consisting of a rotating pendulum and another one at rest (up to quantum fluctuations). As the pendula are not coupled, this state is represented by the tensorial product of the SPP's ground state $|\sigma_0\rangle$ (corresponding to the pendulum at rest) and a superposition of two states $(|\sigma_n\rangle, |\alpha_n\rangle)$ belonging to the same doublet n of the SPP (corresponding to a rotating pendulum). The addition of the two SPP spectra and the construction of the quantum rotobreather $|\Phi\rangle$ is schematically depicted in Fig. 7. The states denoted by $|\sigma\rangle$ ($|\alpha\rangle$) are symmetric (antisymmetric) with respect to the inversion of the momentum:

$$|\Phi\rangle = \frac{1}{\sqrt{2}} |\sigma_0\rangle \otimes (|\sigma_n\rangle + |\alpha_n\rangle). \quad (36)$$

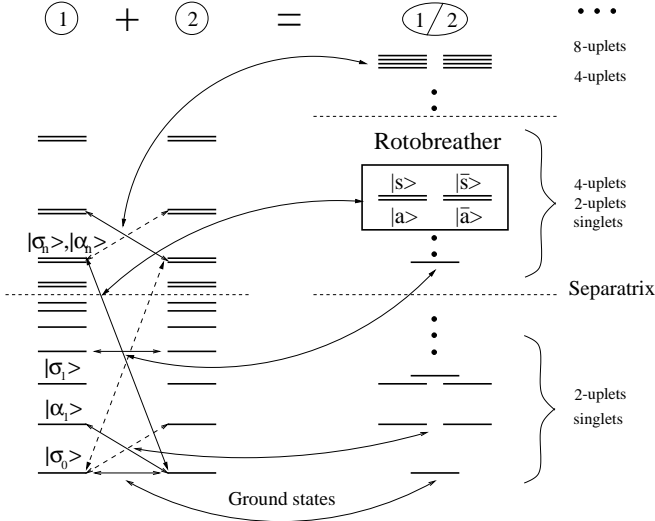


FIG. 7: Schematic representation of the sum of two pendula spectra. Straight solid arrows indicate the levels to be added and dashed arrows indicate the symmetric (permutation) operation. The result is indicated in the global spectrum by a curved arrow. The construction of the quantum rotobreather state $|\Phi\rangle$ is explicitly represented.

In order to obtain the state $|\Phi\rangle$ at $\varepsilon = 0$ as a linear combination of the correctly symmetrized eigenvectors listed in the section III B, we first construct it in terms of the SPP eigenvectors. The correct symmetrization of the tensorial products leads to the following expression of the four possible classes of states:

$$\begin{aligned}
 |s\rangle &= \frac{1}{\sqrt{2}} (|\sigma\rangle \otimes |\sigma'\rangle + |\sigma'\rangle \otimes |\sigma\rangle) \\
 \text{or } \frac{1}{\sqrt{2}} (|\alpha\rangle \otimes |\alpha'\rangle + |\alpha'\rangle \otimes |\alpha\rangle) \\
 |\bar{s}\rangle &= \frac{1}{\sqrt{2}} (|\sigma\rangle \otimes |\sigma'\rangle - |\sigma'\rangle \otimes |\sigma\rangle) \\
 \text{or } \frac{1}{\sqrt{2}} (|\alpha\rangle \otimes |\alpha'\rangle - |\alpha'\rangle \otimes |\alpha\rangle) \\
 |a\rangle &= \frac{1}{\sqrt{2}} (|\sigma\rangle \otimes |\alpha\rangle + |\alpha\rangle \otimes |\sigma\rangle) \\
 |\bar{a}\rangle &= \frac{1}{\sqrt{2}} (|\sigma\rangle \otimes |\alpha\rangle - |\alpha\rangle \otimes |\sigma\rangle) \quad (37)
 \end{aligned}$$

where $|\sigma\rangle, |\sigma'\rangle$ ($|\alpha\rangle, |\alpha'\rangle$) represent any of the symmetric (antisymmetric) SPP eigenvectors.

Using these expressions, $|\Phi\rangle$ is readily written as

$$|\Phi\rangle = \frac{1}{2} (|s\rangle + |\bar{s}\rangle + |a\rangle + |\bar{a}\rangle) \quad (38)$$

where $|s\rangle, |\bar{s}\rangle = (|\sigma_0\rangle \otimes |\sigma_n\rangle \pm |\sigma_n\rangle \otimes |\sigma_0\rangle)/\sqrt{2}$ and $|a\rangle, |\bar{a}\rangle = (|\sigma_0\rangle \otimes |\alpha_n\rangle \pm |\sigma_n\rangle \otimes |\alpha_0\rangle)/\sqrt{2}$. In this anti-continuous limit, we may compute the eigenvalues corresponding to each of the four states which contribute to

$|\Phi\rangle$. We obtain

$$\tilde{E}_s = \tilde{E}_{\bar{s}} = \tilde{E}_{\sigma_0} + \tilde{E}_{\sigma_n} ; \quad \tilde{E}_a = \tilde{E}_{\bar{a}} = \tilde{E}_{\sigma_0} + \tilde{E}_{\alpha_n}. \quad (39)$$

As the expression (39) shows, the absence of any coupling between the pendula is responsible for the true degeneracy of the states whose parity is the same with respect to the momentum reversal symmetry. This follows from the fact that the global spectrum is given by the sum of the SPP spectrum with itself in the anti-continuous limit (cf. Fig. 7). Thus the energy level $\tilde{E}_{\sigma_0} + \tilde{E}_{\sigma_n}$ is obtained in this limit either by adding the energy of the ground state $|\sigma_0\rangle$ of the first pendulum to the energy of the symmetric state $|\sigma_n\rangle$ of the n^{th} doublet of the second pendulum, or by adding the energy of the ground state of the second pendulum to the energy of the symmetric state of the first one.

We have already shown (see 20) that the presence of an onsite potential ($\alpha \neq 0$) lifts the degeneracy of the symmetric and antisymmetric states belonging to the same doublet of the SPP. We may thus compute the splitting between the two pairs of degenerated states ($|s\rangle, |\bar{s}\rangle$) and ($|a\rangle, |\bar{a}\rangle$):

$$\delta_n = \tilde{E}_s - \tilde{E}_a = 2 \frac{\alpha^{2n}}{(2n-1)!^2}. \quad (40)$$

For sufficiently large n this splitting is extremely small and thus the four states making up $|\Phi\rangle$ form a *quadruplet* of nearly degenerated eigenenergies which has been represented in Fig. 7. Notice finally that the inverse of this splitting is directly related to the time taken by the system whose initial state is $|\Phi\rangle$ to reverse its total momentum. As one of the pendula is at rest (up to quantum fluctuations), this means that the pendulum initially rotating in a given sense tunnels into the state which corresponds to the opposite rotation sense on a time scale $\tau_p \sim 1/\delta_n$. This effect is purely quantum.

2. Nonzero coupling ε

As soon as the coupling parameter ε is nonzero the degeneracy of the states ($|s\rangle, |\bar{s}\rangle$) and ($|a\rangle, |\bar{a}\rangle$) of the quadruplet is lifted. Here we are interested in the computation of the corresponding eigenvalues in order to find the splittings which determine the evolution of quantities such as individual energies or momenta of the pendula. If the splittings between the states making up the quantum breather become of the order of the mean level spacing of the spectrum, we may conclude that the breather solution is lost [55].

One possible source of a dramatic increase of the splittings can be a strong overlap of the quantum state with the chaotic layer of the classical system (see e.g. [56] for a general review of the manifestations of classical phase space structures in quantum mechanics). This overlap is generally computed by the mean of a Husimi distribution which is one of the possible phase-space representations

of a quantum state (see e.g. [57]). This distribution is then superposed to the corresponding Poincaré section of the classical system which allows to compute the overlap. This method has for instance been used in the case of a driven bistable system [58]. At the same time these studies have shown that doublet states overlapping up to 70% with the chaotic layer may still possess a small splitting. To avoid misinterpretations, here we will compare the Fourier components of the quantum rotobreather $|\Phi\rangle$, with the Poincaré section of the classical system in the momenta space. The main result will be that the phase space locations of the classical and the quantum rotobreathers are roughly the same.

This direct comparison is possible due to the results obtained in [59] showing that the Husimi distribution of the pendulum problem can be found analytically. It follows that for the pendulum potential, the discrete Fourier representation of the eigenfunctions and their Husimi distributions restricted to the momentum space differ insignificantly.

3. Tunneling of the $|\Phi\rangle$ state

In this section we derive the expressions of some relevant quantities which allow us to follow the time evolution of the initial state $|\Phi\rangle = (|s\rangle + |\bar{s}\rangle + |a\rangle + |\bar{a}\rangle)/2$. This state is formed at $\varepsilon \neq 0$ by the eigenstates which belong to the quadruplet of states. These states in turn are defined by the tensorial product of the ground-state of the SPP spectrum and one of its doublets at the anti-continuous limit. Because $|\Phi\rangle$ is not an eigenstate it evolves in time. In order to visualize this evolution and because we are working in the 2D discrete Fourier space (2DFS), we may compute the time evolution of its momentum. This is done by computing the two functions $\langle\Delta P\rangle = \langle\Phi|\hat{P}_1 - \hat{P}_2|\Phi\rangle$ and $\langle P\rangle = \langle\Phi|\hat{P}_1 + \hat{P}_2|\Phi\rangle$ where \hat{P}_1 and \hat{P}_2 are respectively the momenta operators of the pendula 1 and 2. If the total momentum of the system were conserved (as in the integrable limit $\alpha = 0$), the difference of the momenta $\langle\Delta P\rangle$ would exactly represent the transfer of momentum between the pendula. This is not the case for a nonzero value of α . Although the total momentum $\langle P\rangle$ is in general not conserved, for not too small values of ε it evolves very slowly as compared to $\langle\Delta P\rangle$. We thus may consider that the latter represents the transfer of the excitation from pendulum to pendulum with a good accuracy.

Another quantity of interest is the difference between the individual (or onsite) energies $\langle\Delta H\rangle = \langle\Phi|\hat{H}_1 - \hat{H}_2|\Phi\rangle$ where $\hat{H}_i = \hat{P}_i^2/2 + \alpha(1 - \cos\hat{X}_i)$. As the total energy of the system is conserved, $\langle\Delta H\rangle$ measures the transfer of energy between the pendula.

In order to give a simple expression of the above quantities let us use the two symmetries of permutation and momentum reversal. We denote their respective operators by \mathcal{P} and \mathcal{M} . It is easily shown that they are unitary: $\mathcal{P}^\dagger\mathcal{P} = \mathcal{M}^\dagger\mathcal{M} = \mathbb{1}$ (see e.g. [60]). Moreover, the

following relations hold:

$$\mathcal{M}^\dagger\hat{P}_i\mathcal{M} = -\hat{P}_i \quad ; \quad \mathcal{P}^\dagger\hat{P}_i\mathcal{P} = \hat{P}_j \quad (41)$$

$$\mathcal{M}^\dagger\hat{H}_i\mathcal{M} = \hat{H}_i \quad ; \quad \mathcal{P}^\dagger\hat{H}_i\mathcal{P} = \hat{H}_j \quad (42)$$

$$\mathcal{M}^\dagger\hat{H}_{\text{int}}\mathcal{M} = \hat{H}_{\text{int}} \quad ; \quad \mathcal{P}^\dagger\hat{H}_{\text{int}}\mathcal{P} = \hat{H}_{\text{int}} \quad (43)$$

where $(i, j) \in (1, 2), i \neq j$ and where $\hat{H}_{\text{int}} = \varepsilon(1 - \cos(\hat{X}_1 - \hat{X}_2))$ is the interaction energy term.

Using the fact that the Hilbert space \mathcal{E} associated to the coupled pendula problem can be written as the direct sum $\mathcal{E} = \mathcal{E}_s \oplus \mathcal{E}_{\bar{s}} \oplus \mathcal{E}_a \oplus \mathcal{E}_{\bar{a}}$, any operator may be represented by a 4×4 block-matrix in the basis $(\{|s_i\rangle\}, \{|\bar{s}_j\rangle\}, \{|a_k\rangle\}, \{|\bar{a}_l\rangle\})$ formed by all the states belonging to \mathcal{E}_s first, then all the states belonging to $\mathcal{E}_{\bar{s}}$, etc... in the order described above. From the preceding relations and by using the symmetry properties of the eigenstates, it follows that the relevant operators for our study have the form

$$\hat{P}_{1,2} = \begin{pmatrix} 0 & 0 & P_{as} & \pm P_{\bar{a}s} \\ 0 & 0 & \pm P_{a\bar{s}} & P_{\bar{a}\bar{s}} \\ P_{sa} & \pm P_{\bar{s}a} & 0 & 0 \\ \pm P_{s\bar{a}} & P_{\bar{s}\bar{a}} & 0 & 0 \end{pmatrix} \quad (44)$$

and

$$\hat{H}_{1,2} = \begin{pmatrix} H_{ss} & \pm H_{\bar{s}s} & 0 & 0 \\ \pm H_{s\bar{s}} & H_{\bar{s}\bar{s}} & 0 & 0 \\ 0 & 0 & H_{aa} & \pm H_{\bar{a}a} \\ 0 & 0 & \pm H_{a\bar{a}} & H_{\bar{a}\bar{a}} \end{pmatrix}. \quad (45)$$

We have used the condensed notation $O_{\mu\nu} = \langle\mu|\hat{O}_1|\nu\rangle$ which symbolically represents all the matrix elements of the observable \hat{O}_1 between states of two given subspaces \mathcal{E}_μ and \mathcal{E}_ν . The sign \pm is $+$ for 1 and $-$ for 2. In this basis, the operator \hat{H}_{int} is block-diagonal.

Using the time evolution of the initial state $|\Phi\rangle$

$$|\Phi(t)\rangle = \frac{1}{2} \sum_{\mu} e^{-iE_{\mu}t} |\mu\rangle \quad \text{where } \mu \in \{s, \bar{s}, a, \bar{a}\} \quad (46)$$

we finally obtain

$$\begin{aligned} \langle\Delta P\rangle &= \langle s|\hat{P}_1|\bar{a}\rangle \cos(E_s - E_{\bar{a}})t \\ &+ \langle \bar{s}|\hat{P}_1|a\rangle \cos(E_{\bar{s}} - E_a)t \end{aligned} \quad (47)$$

$$\begin{aligned} \langle P\rangle &= \langle s|\hat{P}_1|a\rangle \cos(E_s - E_a)t \\ &+ \langle \bar{s}|\hat{P}_1|\bar{a}\rangle \cos(E_{\bar{s}} - E_{\bar{a}})t \end{aligned} \quad (48)$$

$$\begin{aligned} \langle\Delta H\rangle &= \langle s|\hat{H}_1|\bar{s}\rangle \cos(E_s - E_{\bar{s}})t \\ &+ \langle a|\hat{H}_1|\bar{a}\rangle \cos(E_a - E_{\bar{a}})t. \end{aligned} \quad (49)$$

Notice that the energy differences occurring in $\langle\Delta H\rangle$ are zero at the anti-continuous limit. No transfer of energy between the pendula occurs due to the fact that they are decoupled. The excitation (and thus the energy) is entirely conserved on its initial site. In this limit we know (in leading order) the value of the splittings $E_s -$

$E_a = E_{\bar{s}} - E_{\bar{a}} = \alpha^{2n}/(2n-1)!^2$ and thus the time taken by the system to reverse its initial momentum: $\tau_p = \pi(2n-1)!^2/\alpha^{2n}$ where n labels the doublet of the rotating pendulum. These splittings also occur in $\langle \Delta P \rangle$. Thus for small ε we can not assign the meaning of a transfer of momentum between the pendula to the time evolution of $\langle \Delta P \rangle$.

In the other integrable limit where $\varepsilon \neq 0$ but $\alpha = 0$, it is also possible to compute the exact spectrum of the system. Notice that the total momentum of the system is strictly conserved in this case. The absence of the onsite potential is also responsible for the degeneracy of the states of different parity concerning the momentum reversal symmetry. We thus have $E_s = E_a$ and $E_{\bar{s}} = E_{\bar{a}}$. It is possible to show (see appendix A) that the splitting $E_s - E_{\bar{s}} = (a_n(-2\varepsilon) - b_n(-2\varepsilon))/4$ which in leading order gives $|E_s - E_{\bar{s}}| = 2(\varepsilon/2)^n/(n-1)!^2$ where n is the label of the doublet of the initially rotating pendulum. The time taken by the system to transfer its excitation from one site to the second one is $\tau_e = \pi(n-1)!^2/2(\varepsilon/2)^n$ in this limit. By comparing τ_e with τ_p we observe that for large enough n , $\tau_p \gg \tau_e$ holds, regardless the values of ε and α . This indicates that in general transfer of energy (and momentum) from site to site will be a much faster process than the process of total momentum reversal.

When α and ε are both nonzero, the different splittings have to be calculated numerically by following the evolution of the quadruplet as a function of the coupling ε . This is the purpose of the following section.

4. Following the quadruplet

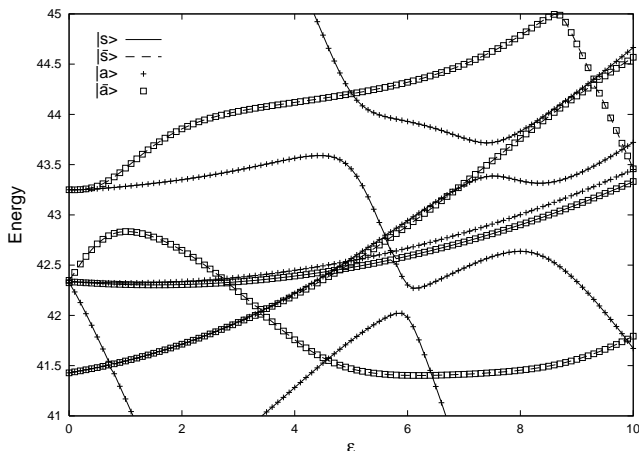


FIG. 8: Evolution of a part of the spectrum as a function of the coupling ε . The onsite parameter is $\alpha = 5$. Energies are rescaled according to $\tilde{E} = 2(E - 2\alpha - \varepsilon)$. The quadruplet under investigation starts at an energy $\tilde{E} \simeq 41.43$. It corresponds to a state formed of the ground-state of the SPP and the doublet $n = 7$.

In Fig. 8, we have plotted the evolution of a part of the global spectrum of the coupled pendula as a function

of the coupling ε . The onsite parameter is $\alpha = 5$. The energies of the different classes of states have been represented by different lines and symbols. The quadruplet which represents the levels of the states $\{|s\rangle, |\bar{s}\rangle, |a\rangle, |\bar{a}\rangle\}$ from which $|\Phi\rangle$ is formed, has an energy $\tilde{E} \simeq 41.43$ at $\varepsilon = 0$. This corresponds to a quadruplet made of the ground-state of the SPP and the doublet $n = 7$ at the anti-continuous limit. Indeed, by using (17) and (19), we obtain $\tilde{E}_1^d \simeq 49 + 50/195$ and $E_0 \simeq \sqrt{5} - 1/16 \Rightarrow \tilde{E}_0 \simeq \sqrt{5} - 1/16 - 10$. The sum of these energies gives $\tilde{E} \simeq 41.43$. At $\varepsilon = 1$ the quadruplet energy is $\tilde{E} \simeq 41.54$. This corresponds to $E \simeq 31.77$ which precisely represents the energy of the classical rotobreather presented in the section III A.

At slightly larger energy in the spectrum we observe an octuplet. It consists of states mixing two neighboring doublets, namely $n = 4$ and $n' = 5$. Its energy is around $\tilde{E} \simeq 42.3$ which can be computed also by using (19). The reason for the occurrence of this octuplet is depicted in Fig. 7. By combining the two states of the doublet n with those of n' we obtain four different (although nearly degenerated) levels of energy. But there are two ways to attribute these doublets to the pendula 1 and 2 (represented by the solid and dashed arrows in Fig. 7). We thus obtain two identical quadruplets which yield an octuplet. Finally, the visible cluster of levels at $\tilde{E} \approx 43.25$ corresponds to a quadruplet made of the combination of a single symmetric state (the last one situated below the separatrix $\tilde{E}_{\text{sep}} = 2\alpha = 10$) with the doublet $n = 6$.

From a general point of view, the evolution of the energy levels of a spectrum as a function of a given parameter (here ε) can be compared to the time evolution of a gas of particles obeying dynamical laws of the Calogero-Moser system type ([61]-[64]). This system is Hamiltonian and the interaction between particles (eigenvalues) is strongly repulsive at short distances. This gives rise to avoided crossings. Nevertheless, in the presence of symmetries, the different parity sectors decouple from each other and thus, do not interact [65]. As a result, the four sectors $\{s, \bar{s}, a, \bar{a}\}$ evolve individually according to the Calogero-Moser dynamics but do not interact with each other. Thus they may cross. Such a crossing is observed in Fig. 8 in the vicinity of the point $(\varepsilon = 5, \tilde{E} = 44)$. Fig. 8 also shows the pairing of eigenvalues whose momentum related parities are complementary. For instance eigenvalues of the s sector cluster with eigenvalues of the a or \bar{a} sectors. They are indeed quasi-indistinguishable. The reason is that the influence of the onsite potential becomes weak and thus the corresponding splittings small as the energy becomes sufficiently high.

By following the quadruplet which starts at $\tilde{E} \simeq 41.43$, we observe that it first survives an avoided crossing with one $(|s\rangle, |a\rangle)$ pair ($\varepsilon \sim 0.7$). Then it survives again another one with two $(|\bar{s}\rangle, |\bar{a}\rangle)$ states and starts to split into two pairs $(|s\rangle, |a\rangle)$ and $(|\bar{s}\rangle, |\bar{a}\rangle)$ after a collision with a quasi-quadruplet which originates from the octuplet at $\tilde{E} \simeq 42.3$. Finally, in the vicinity of $\varepsilon = 7.5$, the $(|\bar{s}\rangle, |\bar{a}\rangle)$

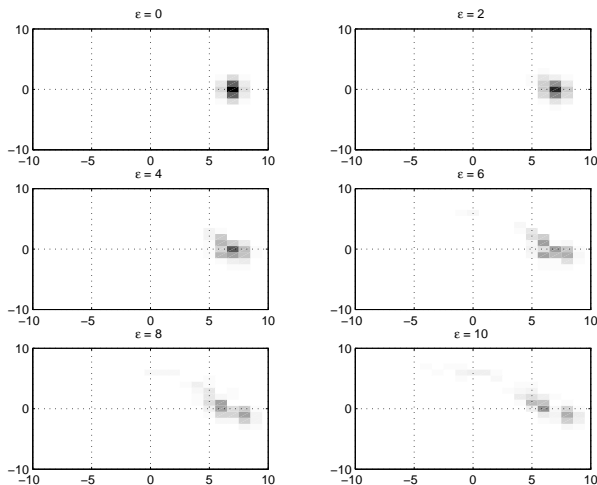


FIG. 9: Evolution of $|\Phi\rangle$ ($|\Phi_{m,n}|^2$) as the coupling strength ε increases. Each picture represents the 2D Fourier space, $p_1(m)$ along the x axis and $p_2(n)$ along the y axis. The value of each component $|\Phi_{m,n}|^2$ is represented by its gray level from white (0) to black (~ 0.3).

pair seems to join a new $(|s\rangle, |a\rangle)$ pair but remains clearly separated from it. The fact that pairs of permutationally related eigenvalues may survive avoided crossings is already known and may for instance be observed in the case of the trimer problem ([55],[24]).

In order to see the progressive evolution of our initial state $|\Phi\rangle$ as the coupling increases, we have plotted snapshots of its evolution for different values of ε (Fig. 9). Each picture represents the 2D discrete Fourier space. The x -axis represents the coordinate $m \in \mathbb{Z}$ related to the momentum of the first pendulum p_1 and the y -axis, $n \in \mathbb{Z}$ related to p_2 . The $|\Phi\rangle$ state has been computed on a square lattice of 41×41 Fourier components. For clarity only a 21×21 lattice has been displayed. We observe that the state $|\Phi\rangle$ remains almost unchanged for $0 \leq \varepsilon \leq 2$. The excitation is well localized in the 2D Fourier space. The average momentum $\langle \hat{P}_1 \rangle = \sum_{m,n} m |\Phi_{m,n}|^2$, which defines the projection of the excitation "center" on the x -axis, is large and makes the first pendulum "rotating" whereas $\langle \hat{P}_2 \rangle = \sum_{m,n} n |\Phi_{m,n}|^2$ is small and makes the second pendulum "oscillating". The quotes indicate that this correspondence refers to an interpretation in terms of the classical system. As ε becomes larger than 4, the state starts to spread on the lattice and does not correspond to a "coherent" excitation anymore. A plot of the Poincaré section of the classical system at $\varepsilon = 6$ with an energy corresponding to the one of $|\Phi\rangle$ has shown the allowed region of the Fourier space to be chaotic (except in the vicinity of the in-phase and out-of-phase motion and in a tiny region where the classical rotobreather still exists). This means that any small perturbation of the initial conditions of the classical rotobreather leads to a chaotic trajectory. We verify in this particular example

that the strong overlap of the chaotic sea with the quantum state leads to large splittings of tunneling pairs (here $(|s\rangle, |\bar{s}\rangle)$ and $(|a\rangle, |\bar{a}\rangle)$).

5. Evolution of the splittings with ε

To provide quantitative results concerning the behavior of the different splittings involved in the expressions (47) as ε increases, we have computed them over the same range of values. The result is presented in Fig. 10. It always concerns the state $|\Phi\rangle$ obtained from the quadruplet of preceding section. Notice that for the sake of clarity, only three of the six possible splittings have been displayed on the figure. The omitted splittings behave very similarly according to the symmetry properties of the involved states. Each of the displayed splittings corresponds to a given tunneling process as specified in the figure. After a crossing value $\varepsilon \simeq 0.15$, the graph basically consists of two curves. One is related to the momentum or energy transfer between the pendula and another one is related to the reversal of the total momentum of the system. This means that the upper curve is related to the transfer of the excitation from a general point of view (energy or momentum). The lower curve represents a process (the global momentum reversal) which is not associated to any kind of excitation transfer between the pendula but only to a global modification of the system. It has no relation with the tunneling of the quantum rotobreather from site to site.

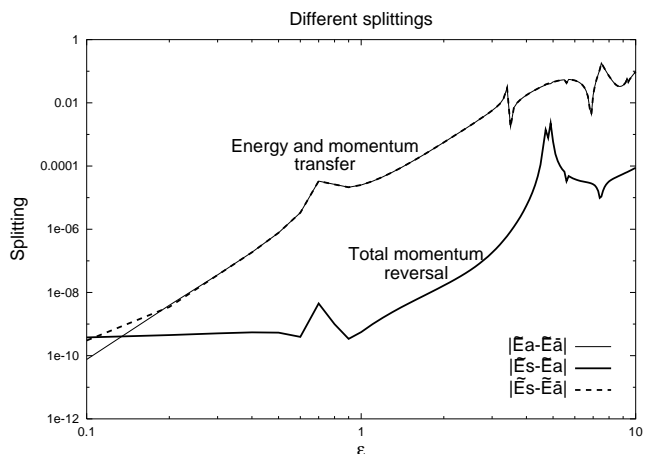


FIG. 10: Dependence of different splittings of the quadruplet whose energy at $\varepsilon = 0$ is $\bar{E} \simeq 41.43$ on ε . Only three of them have been displayed, each being associated with a given tunneling process. The splittings are given in terms of the rescaled energy $\Delta \bar{E} = 2\Delta E$.

Note that at the anti-continuous limit, the energies of the states $|a\rangle$ ($|s\rangle$) and $|\bar{a}\rangle$ ($|\bar{s}\rangle$) are identical. The splitting which corresponds to the energy transfer ($|\bar{E}_a - \bar{E}_{\bar{a}}|$ in the figure) is thus zero. This explains the behavior of the corresponding (thin solid) curve, in logarithmic

scale, which decreases regularly with ε . Moreover, due to this degeneracy, all the remaining splittings are equal and given by (40). For the $|\Phi\rangle$ state we obtain $\delta_7 \simeq 3.15 \cdot 10^{-10}$ which corresponds to the saturation value obtained numerically for $|\tilde{E}_s - \tilde{E}_a|$ and $|\tilde{E}_s - \tilde{E}_{\bar{a}}|$ (thick solid and dashed lines).

The splittings depend smoothly on ε except for values of the coupling where crossings and avoided crossings take place (see Fig. 8). The first crossing involves the quadruplet states $\{|s\rangle, |a\rangle, |\bar{s}\rangle, |\bar{a}\rangle\}$ and a $(|s'\rangle, |a'\rangle)$ pair at $\varepsilon \simeq 0.73$. Avoided crossings occur between $(|s\rangle, |s'\rangle)$ and $(|a\rangle, |a'\rangle)$ pairs and are responsible for the peaks appearing in the three splittings. The case of the second crossing ($\varepsilon \simeq 3.30$) is slightly different. This avoided crossing concerns the $(|\bar{s}\rangle, |\bar{s}'\rangle)$ and $(|\bar{a}\rangle, |\bar{a}'\rangle)$ pairs. The splitting $|\tilde{E}_s - \tilde{E}_a|$ behaves smoothly whereas the two others exhibit spikes due to the collision. This follows from the fact that $|\tilde{E}_s - \tilde{E}_a|$ does not contain any contribution of states interacting with the colliding pair. Note that the spikes observed in such crossings may have different forms according to the exact realization of the collision and the specific splitting under consideration [24].

Finally, when the coupling parameter becomes larger than 5, the splittings corresponding to the transfer of the excitation between the pendula start to be of the same order as the mean spacing in the spectrum ($1/\pi$ here as shown in (34)). This is the signature of the disappearance of the quantum rotobreather since no quantum state is able to keep the energy on a given pendulum during a sufficiently long time at the considered energy level.

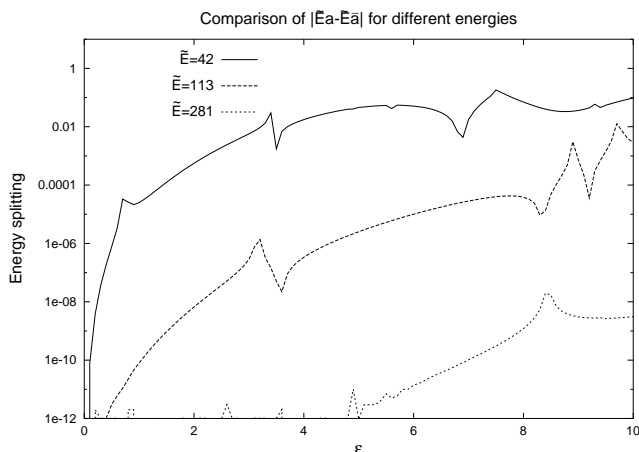


FIG. 11: Dependence of the splitting governing the energy tunneling on ε for different quadruplet energies. The three curves correspond to quadruplets starting from a ground state and a doublet at $\varepsilon = 0$. The respective labels are $m = 7, 11$ and 17 . The corresponding energies at $\varepsilon = 0$ are $\tilde{E} = 41.43, 113.3$ and 281.2 .

We conclude this section by discussing the dependence of the splitting governing the energy transfer on the quadruplet energy (Fig. 11). As expected the splittings

decrease with increasing quadruplet energy. This can be qualitatively understood by referring to the analytical expression of the splitting at $\alpha = 0$. Indeed, taking into account the slow change of the quadruplet energy with ε , $\tilde{E}_{m,0} \simeq m^2 + \varepsilon^2/(m^2 - 1)$, we may directly replace m by $\sqrt{\tilde{E}_{m,0}}$ in the expression of the splitting. We thus obtain $\Delta(\tilde{E}, \alpha = 0) \simeq 4(\varepsilon/2)\sqrt{\tilde{E}}/\Gamma(\sqrt{\tilde{E}})^2$ which gives a rapidly decreasing function of the quadruplet energy for values of $\varepsilon \ll \tilde{E}$.

IV. SUMMARY AND CONCLUDING REMARKS

In this paper, after a brief review of the essential results of the single pendulum problem, we have used a two coupled pendula model to show the possibility of constructing a quantum state $|\Phi\rangle$ whose properties are similar to those of a classical rotobreather. This state has been built in a very similar manner to those used in the corresponding classical system, namely, by starting from a state which mimics the behavior of a rotating pendulum decoupled from another one at rest at the anti-continuous limit. Four states, each belonging to a different symmetry sector, are shown to be necessary to form it. By switching on the coupling between the pendula, we follow the resulting evolution of the quadruplet and monitor the different splittings. Each of them can be shown to be associated to a given tunneling process according to the involved states.

In general, we have seen that two processes have to be distinguished. The first concerns the tunneling (or transfer) of the initial excitation (energy) between the pendula which corresponds to a tunneling of the quantum rotobreather $|\Phi\rangle$ between neighboring sites. This tunneling effect is associated to the permutation symmetry present in the system. The second tunneling effect relies on another symmetry due to the invariance of the system to a reversal of its total momentum. This symmetry already appears in the single pendulum problem where it is responsible for the occurrence of doublets of nearly degenerated states at sufficiently high energy (above the separatrix). This second tunneling effect takes a time which is orders of magnitude larger than the time of the excitation transfer between pendula (except for very small coupling values).

By progressively increasing the pendula coupling, we have shown that the quadruplet under investigation may survive crossings (or avoided crossings) with other states. Nevertheless, for large enough coupling, the nearly degenerated states of different permutation symmetry parities separate sufficiently from each other, leading to splittings of order of the mean level spacing in the spectrum. This situation corresponds classically to a large chaotization of the phase space at the considered energy level and thus to a strong overlap of the quantum state with the chaotic layer surrounding the quasi-regular island where

the classical rotobreather is located. The disappearance of the quantum rotobreather can be interpreted by the fact that the corresponding state is no more able to keep the excitation in a given pendulum for a long time as compared to the typical oscillation time of the system.

To conclude this paper, we would like to comment on the relation between the classical and the quantum (roto)breathers. An essential ingredient for the existence of a quantum breather is the appearance of bands of nearly degenerated eigenstates whose bandwidth remain very small as the coupling increases. Nevertheless, the general method employed to construct the quantum breather by starting from the anti-continuous limit may be used as well for a chain of N purely harmonic oscillators (with a harmonic coupling). As this chain cannot possess any kind of classical breathers, what prevents quantum breathers from existing on such a chain? To answer this question, we compute the bandwidth corresponding to a local excitation of n bosons close to the anti-continuous limit. We obtain $\Delta E_n = n(\sqrt{\omega^2 + 4\varepsilon} - \omega)$, ω being the oscillator frequency and ε the coupling. This shows that the bandwidth becomes large as the mean energy of the band $E_n \sim n\omega$ does. Moreover, the density of states scales like $g(E) \sim E^{N-1}$ (see the introduction) and the product $g(E_n)\Delta E_n \rightarrow \infty$ as $E \rightarrow \infty$. This shows that like the classical harmonic chain, the quantum system cannot support quantum breathers.

A second comment concerns the "classical-like" behavior of the quantum breather. By defining the latter as a superposition of the eigenstates making up a single band, its time evolution is de facto restricted to these states. The fine structure of the band thus provides the only available frequencies of this evolution. As the corresponding splittings are very small, none of them is related to the classical breather frequency. These frequencies only concern the tunneling of the excitation from site to site. On the other hand, the individual energies of particles making up a classical breather, for example, oscillate around their mean value at the breather frequency. Where does such a frequency appear in the quantum system? It turns out that this frequency is naturally recovered by considering quantum states which display an excitation similar to the quantum breather but which are not restricted to a single band. We have verified in our system that a coherent state parametrized by the average phases and momenta of the quantum rotobreather $|\Phi\rangle$ excites mainly the quadruplets separated by an energy difference which corresponds approximately to the classical rotobreather frequency. The interaction between quadruplets is thus responsible for the "classical-like" time behavior of averaged observables (like individual energies). This should generalize to nonlinear systems with more than two degrees of freedom where we expect interactions between bands to play a similar role as the interaction between quadruplets in our system.

APPENDIX A: COUPLED ROTORS

In this appendix, we solve the problem of two coupled rotors, i.e. the limit of the two coupled pendula when the onsite parameter α is equal to zero. In this case, the system defined by the Hamiltonian (29) is integrable. Indeed,

$$H_{\text{cr}} = \frac{1}{2}(p_1^2 + p_2^2) + \varepsilon(1 - \cos(x_1 - x_2)) \quad (\text{A1})$$

Let $s = (x_1 + x_2)/2$ and $d = (x_1 - x_2)/2$. Then the classical equations of motion reads

$$\ddot{s} = 0 \quad (\text{A2})$$

$$\ddot{d} + \varepsilon \sin(2d) = 0 \quad (\text{A3})$$

The system decouples and consists of a free rotor for the center of mass motion and a pendulum for the relative coordinate $2d$ (with an "onsite" parameter 2ε).

Let us turn to the associated quantum problem. The Hamiltonian (A1) gives rise to the time independent Schrödinger equation

$$\left[-\frac{1}{2}(\partial_{x_1}^2 + \partial_{x_2}^2) + \varepsilon(1 - \cos(x_1 - x_2)) - E \right] \psi(x_1, x_2) = 0 \quad (\text{A4})$$

which yields (after the change of variables defined above)

$$\left[-\frac{1}{4}(\partial_s^2 + \partial_d^2) + \varepsilon(1 - \cos(2d)) - E \right] \tilde{\psi}(s, d) = 0 \quad (\text{A5})$$

where $\tilde{\psi}(s, d) = \psi(x_1, x_2)$. Because of the 2π -periodicity of $\psi(x_1, x_2)$ in each of its variables we may expand it as a double Fourier series:

$$\begin{aligned} \psi(x_1, x_2) &= \frac{1}{2\pi} \sum_{m, n \in \mathbb{Z}^2} \psi_{m, n} \exp(i(mx_1 + nx_2)) \quad (\text{A6}) \\ &= \frac{1}{2\pi} \left\{ \sum_{\sigma, \delta \in (2\mathbb{Z})^2} \tilde{\psi}_{\sigma, \delta}^{(e)} \exp(i(\sigma s + \delta d)) \right. \\ &\quad \left. + \sum_{\sigma, \delta \in (2\mathbb{Z}+1)^2} \tilde{\psi}_{\sigma, \delta}^{(o)} \exp(i(\sigma s + \delta d)) \right\} \quad (\text{A7}) \\ &= \tilde{\psi}(s, d) \end{aligned}$$

where we have defined $\sigma = m + n$ and $\delta = m - n$ and where the notations $\sigma, \delta \in (2\mathbb{Z})^2$ and $\sigma, \delta \in (2\mathbb{Z}+1)^2$ indicate respectively that σ, δ have to be both even numbers or both odd numbers. Moreover, $\tilde{\psi}_{\sigma, \delta}^{(e)} = \psi_{(\sigma+\delta)/2, (\sigma-\delta)/2}$ for σ, δ both even (reason of the superscript (e)) and similarly $\tilde{\psi}_{\sigma, \delta}^{(o)} = \psi_{(\sigma+\delta)/2, (\sigma-\delta)/2}$ for σ, δ both odd. It follows that the first term in (A7) is a π -periodic function in each of the variables s or d whereas the second one is 2π -periodic.

Notice further that because the potential only depends on d , (A5) decouples to give

$$\left[-\frac{1}{2}\partial_s^2 - 2E_s\right]\tilde{\psi}_s(s) = 0 \quad (\text{A8})$$

$$\left[-\frac{1}{2}\partial_d^2 + 2\varepsilon(1 - \cos(2d)) - 2E_d\right]\tilde{\psi}_d(d) = 0 \quad (\text{A9})$$

where $\tilde{\psi}(s, d) = \tilde{\psi}_s(s)\tilde{\psi}_d(d)$ and $E = E_s + E_d$.

The last equation of (A8) is a Mathieu equation with a characteristic value a and a parameter q defined by

$$a = 4(E_d - \varepsilon) \quad \text{and} \quad q = -2\varepsilon \quad (\text{A10})$$

Taking into account the preceding remarks concerning the periodicity as well as the two possible parities (odd or even) of the solutions, we finally get

$$E_s^\sigma = \frac{1}{4}\sigma^2 \quad \text{and} \quad E_d^\delta = \frac{1}{4}\left(\begin{matrix} a \\ b \end{matrix}\right)_\delta(q) + \varepsilon \quad (\text{A11})$$

where $\sigma, \delta \in \mathbb{Z}^2$ have to have the same parity (even or odd) and where we have introduced a spinor notation

$$\left(\begin{matrix} f \\ g \end{matrix}\right)_\mu(z) = \begin{cases} f_\mu(z) & \text{if } \mu \geq 0 \\ g_{|\mu|}(z) & \text{if } \mu < 0 \end{cases} \quad (\text{A12})$$

For the usual notation of the Mathieu equation see [47]. By defining the rescaled energy by $\tilde{E} = 2(E - \varepsilon)$ and using the quantum numbers m, n we finally get the following expression for the spectrum of the coupled rotors

$$\tilde{E}_{m,n} = \frac{1}{2}\left((m+n)^2 + \left(\begin{matrix} a \\ b \end{matrix}\right)_{(m-n)}(-2\varepsilon)\right) \quad (m, n) \in \mathbb{Z}^2 \quad (\text{A13})$$

It follows $\tilde{E}_{m,n} = \tilde{E}_{-n,-m}$. Thus all the levels are twofold degenerated except when $m = -n$, which corresponds to a total momentum of the system equal to zero. Notice that, when $\varepsilon \rightarrow 0$, the characteristic values converge to $(m-n)^2$ and we recover the free rotors spectrum $\tilde{E}_{m,n} = m^2 + n^2$. Moreover, at sufficiently high momenta differences $|m-n| \gg \sqrt{\varepsilon}$, the energies $\tilde{E}_{m,n}$ and $\tilde{E}_{n,m}$ become nearly degenerated. Their splitting, computed by means of (21) gives

$$\Delta E_{|m-n|} = \frac{1}{2}\Delta \tilde{E}_{|m-n|} = 2\frac{(\varepsilon/2)^{|m-n|}}{(|m-n|-1)!^2} \quad (\text{A14})$$

The eigenfunctions corresponding to the spectrum (A13) may be expressed according to their symmetry sectors by

$$\psi^{(m,n)}(x_1, x_2) = \mathcal{N}_\sigma \left(\begin{matrix} C \\ S \end{matrix}\right)_\sigma(s) \left(\begin{matrix} ce \\ se \end{matrix}\right)_\delta(d; q) \quad (\text{A15})$$

where the normalization factor \mathcal{N}_σ is $1/\pi$ for $\sigma \neq 0$ and $1/\sqrt{2\pi}$ if $\sigma = 0$ and where σ, δ, s and d have already been defined as functions of m, n, x_1 and x_2 . $C_\sigma(s) = \cos(\sigma s)$ and $S_\sigma(s) = \sin(\sigma s)$. With this notation, the correspondence between the symmetry sectors and the values of σ and δ are

$$\begin{aligned} |s\rangle &\Rightarrow (\sigma \geq 0; \delta \geq 0) & ; & \quad |a\rangle \Rightarrow (\sigma < 0; \delta \geq 0) \\ |\bar{s}\rangle &\Rightarrow (\sigma < 0; \delta < 0) & ; & \quad |\bar{a}\rangle \Rightarrow (\sigma \geq 0; \delta < 0) \end{aligned}$$

-
- [1] A.A. Ovchinnikov, Localized long-lived vibrational states in molecular crystals, *Zh. Eksp. Teor. Fiz.* **57**, p. 263-270 (1969) (Eng. transl. *Sov. Phys. JETP* **30**, 1, p. 147-150 (1970))
- [2] M.M. Bogdan, A.M. Kosevich, Quantization of self-localized vibrations in a one-dimensional anharmonic chain, *Sov. J. Low Temp. Phys.* **2**, 6, p. 391-395 (1976)
- [3] F. Fillaux, C.J. Carlile, Inelastic-neutron-scattering study of methyl tunneling and the quantum sine-Gordon breather in isotopic mixtures of 4-methyl-pyridine at low temperature, *Phys. Rev. B* **42**, 10, p. 5990-6006 (1990)
- [4] L. Bernstein, J.C. Eilbeck and A.C. Scott, The quantum theory of local modes in a coupled system of nonlinear oscillators, *Nonlinearity* **3**, p. 293-323 (1990)
- [5] F. Fillaux, C.J. Carlile, G.J. Kearley, Inelastic-neutron-scattering study at low temperature of the quantum sine-Gordon breather in 4-methyl-pyridine with partially deuterated methyl groups, *Phys. Rev. B* **44**, 22, p. 12280-12293 (1991)
- [6] M. Salerno, A new method to solve the quantum Ablowitz-Ladik system, *Phys. Lett. A* **162**, p. 381-384 (1992)
- [7] M. Salerno, Quantum deformations of the discrete nonlinear Schrödinger equation, *Phys. Rev. A* **46**, 11, p. 6856-6859 (1992)
- [8] L.J. Bernstein, Quantizing a self-trapping transition, *Physica D* **68**, p. 174-170 (1993)
- [9] E. Wright, J.C. Eilbeck, M.H. Hays, P.D. Miller and A.C. Scott, The quantum discrete self-trapping equation in the Hartree approximation, *Physica D* **69**, p. 18-32 (1993)
- [10] J.C. Eilbeck, H. Gilhøj and A.C. Scott, Solitons bands in anharmonic quantum lattices, *Phys. Lett. A* **172**, p. 229-235 (1993)
- [11] A.C. Scott, J.C. Eilbeck and H. Gilhøj, Quantum lattice solitons, *Physica D* **78**, p. 194-213 (1994)
- [12] S. Aubry, S. Flach, K. Kladko and E. Olbrich, Manifestation of classical bifurcation in the spectrum of the integrable quantum dimer, *Phys. Rev. Lett.* **76**, 10, p. 1607-1610 (1996)
- [13] W.Z. Wang, J. Tinka Gammel, A.R. Bishop and M.I.

- Salkola, Quantum breathers in a nonlinear lattice, *Phys. Rev. Lett.* **76**, 19, p. 3598-3601 (1996)
- [14] S. Aubry, Breathers in nonlinear lattices: Existence, linear stability and quantization, *Physica D* **103**, p. 201-250 (1997)
- [15] S. Flach, C.R. Willis, Discrete breathers, *Phys. Rep.* **295**, p.181-264 (1998)
- [16] W.Z. Wang, A.R. Bishop, J. Tinka Gammel and R.N. Silver, Quantum breathers in electron-phonon systems, *Phys. Rev. Lett.* **80**, 15, p. 3284-3287 (1998)
- [17] F. Fillaux, C.J. Carlile, G.J. Kearley, Inelastic-neutron-scattering study of the sine-Gordon breather interactions in isotopic mixtures of 4-methyl-pyridine, *Phys. Rev. B* **58**, 17, p. 11416-11419 (1998)
- [18] V. Fleurov, R. Schilling and S. Flach, Tunneling of a quantum breather in a one-dimensional chain, *Phys. Rev. E* **58**, 1, p. 339-346 (1998)
- [19] B.I. Swanson, J.A. Brozik, S.P. Love, G.F. Strouse, A.P. Shreve, A.R. Bishop, W.Z. Wang. and M.I. Salkola, Observation of intrinsically localized modes in a discrete low-dimensional material, *Phys. Rev. Lett.* **82**, 16, p. 3288-3291 (1999)
- [20] K. Kladko, J. Malek and A.R. Bishop, Intrinsic localized modes in the charge-transfer solid PtCl, *J. Phys.: Condens. Matter* **11**, 39, p. L415-L422 (1999)
- [21] H. Fehske, G. Wellein, H. Büttner, A.R. Bishop and M.I. Salkola Local mode behavior in quasi-1D CDW systems, *Physica B* **281 & 282**, p. 673-674 (2000)
- [22] A.C. Scott, Nonlinear science, Emergence and dynamics of coherent structures, *Oxford applied and engineering mathematics*, Oxford university press, chap. 8 (2000)
- [23] R.S. MacKay, Discrete breathers: classical and quantum, *Physica A* **288**, p. 174-198 (2000)
- [24] S. Flach, V. Fleurov, A.A. Ovchinnikov, Tunneling of localized excitations: giant enhancement due to fluctuations, *Phys. Rev. B* **63**, 094304, (2001)
- [25] S. Flach and Y. Zolotaryuk, Discrete Breathers in Condensed Matter, *Adv. in Solid State Phys.* **41**, p. 315-327, (2001)
- [26] N.K. Voulgarakis, G. Kalosakas, A.R. Bishop and G.P. Tsironis, Multiquanta breather model for PtCl, *Phys. Rev. B* **63**, 094304, (2001)
- [27] S. Flach, Conditions on the existence of localized excitations in nonlinear discrete systems, *Phys. Rev. E* **50**, 4, p. 3134-3142 (1994)
- [28] R.S. MacKay and S. Aubry, Proof of the existence of breathers for time-reversible or Hamiltonian networks of weakly coupled oscillators, *Nonlinearity* **7**, 6, p. 1623-1643 (1994)
- [29] J.L. Marin, S. Aubry, Breathers in nonlinear lattices: numerical calculation from the anticontinuous limit, *Nonlinearity* **9**, p.1501-1528 (1996)
- [30] G. James, Existence of breathers on FPU lattices, *C. R. Acad. Sci. Paris* **332**, Série I, p.581-586, (2001)
- [31] S. Flach, Existence of localized excitations in nonlinear Hamiltonian lattices, *Phys. Rev. E* **51**, 2, p. 1503-1507 (1995)
- [32] S. Aubry, G. Kopidakis and V. Kadelburg, Variational proof for hard discrete breathers in some classes of Hamiltonian dynamical systems, *DCDS-B* **1**, 3, p. 271-298 (2001)
- [33] A.J. Sievers and S. Takeno, Intrinsic localized modes in anharmonic crystals *Phys. Rev. Lett.* **61**, 8, p. 970-973 (1988)
- [34] S. Flach, Breathers on lattices with long range interaction, *Phys. Rev. E* **58**, 4, p. R4116-R4119 (1998)
- [35] B. Dey, M. Eleftheriou, S. Flach and G.P. Tsironis, Shape profile of compact-like discrete breathers in nonlinear dispersive lattice systems, (To be published)
- [36] S. Flach, K. Kladko and R.S. MacKay, Energy thresholds for discrete breathers in one-, two-, and three-dimensional lattices, *Phys. Rev. Lett.* **78**, 7, p. 1207-1210 (1997)
- [37] S. Aubry and G. Kopidakis, Aspects of discrete breathers and new directions, *arXiv:cond-mat/0102162* (To be published in "Nonlinearity and Disorder: Theory and Applications." *Proc. NATO ARW*) (2001)
- [38] A.A. Ovchinnikov, N.S. Erikhman and K.A. Pronin, Vibrational-Rotational Excitations in Nonlinear Molecular Systems, *Kluwer academic / Plenum publishers*, New-York (2001)
- [39] K. Svenson, L. Bengtsson, J. Bellman, M. Hassel, M. Persson and S. Andersson, Two-dimensional quantum rotation of adsorbed H₂, *Phys. Rev. Lett.* **83**, 1, p. 124-127 (1999)
- [40] C.M. Brown, T. Yildirim, D.A. Neumann, M.J. Heben, T. Gennett, A.C. Dillon, J.L. Alleman, J.E. Fischer, Quantum rotation of hydrogen in single-wall carbon nanotubes, *Chem. Phys. Lett.* **329**, p. 311-316 (2000)
- [41] M. Havighorst, M. Prager, Ammonia tunnelling in Hofmann clathrates: consistent description by internal and center of mass quantum rotation, *Chem. Phys. Lett.* **250**, p. 232-237 (1996)
- [42] J. Colmenero, R. Mukhopadhyay, A. Alegria and B. Frick, Quantum rotational tunneling of Methyl groups in polymers, *Phys. Rev. Lett.* **80**, 11, p. 2350-2353 (1998)
- [43] J. Colmenero, A.J. Moreno, A. Alegria, R. Mukhopadhyay, and B. Frick, Methyl groups dynamics in glassy polymers by neutron scattering: from classical to quantum motions, *Physica B* **276-278**, p. 322-325 (2000)
- [44] W. Wegener, C. Bostoen and G. Coddens, Nearly free quantum rotations of ammonia groups in Ni-Ni-Bz(d₆) Hofmann clathrate, *J. Phys.: Condens. Matter* **2**, p. 3177-3185 (1990)
- [45] M. Kolarschik, G. Voll, Rotational tunnelling of a C₃-symmetric rotor with non-fixed axis in a C₄-symmetric cage, *Physica B* **222**, p. 1-15 (1996)
- [46] R. Aldrovandi, P. Leal Ferreira, Quantum pendulum, *Am. J. Phys.* **48**, 8, p. 660-4 (1980)
- [47] M. Abramowitz, I.A. Stegun, Handbook of mathematical functions, Dover eds. (1972)
- [48] J.C. Ross, H.W. Capel, Fractional revivals of coherence in quantum mechanical oscillators, *Physica A* **287**, p. 217-258 (2000)
- [49] P. A. Braun, Discrete semiclassical methods in the theory of Rydberg atoms in external fields, *Rev. Mod. Phys.* **65**, 1, p. 115-161 (1993)
- [50] A. Garg, Application of the discrete Wentzel-Kramers-Brillouin method to spin tunneling, *J. Math. Phys.* **39**, 10, p. 5166-5179 (1998)
- [51] M. P. Marder, Condensed Matter Physics, *Wiley-Interscience Publication* p. 160-162 (2000)
- [52] S. Takeno and M. Peyrard, Nonlinear rotating modes: Green's-function solution, *Phys. Rev. E* **55**, 2, p. 1922-1928 (1997)
- [53] J. Brüderin, Einführung in die analytische Zahlentheorie, *Springer Verlag*, p. 44-45 (1995)
- [54] P. Cvitanovic et al., Classical and quantum chaos,

www.nbi.dk/ChaosBook, version **8.1.2** (2001)

- [55] S. Flach and V. Fleurov, Tunneling in the nonintegrable trimer - a step towards quantum breathers, *J. Phys. Condens. Matter* **9**, p.7039-7061 (1997)
- [56] O. Bohigas, S. Tomsovic and D. Ullmo, Manifestations of classical phase space structures in quantum mechanics, *Phys. Rep.* **223**, 2, p.43-133 (1993)
- [57] Hai-Woong Lee, Theory and application of the quantum phase-space distribution functions, *Phys. Rep.* **259**, p.147-211 (1995)
- [58] R. Utermann, T. Dittrich and P. Hänggi, Tunneling and the onset of chaos in a driven bistable system, *Phys. Rev. E* **49**, p.273-280 (1994)
- [59] G. Torres-Vega, J.D. Morales-Guzman and A. Zúñiga-Segundo, Special functions in phase space: Mathieu functions, *J. Phys. A: Math. Gen.* **31**, p.6725-6739 (1998)
- [60] C. Cohen-Tannoudji, B. Diu, F. Laloë, Quantum mechanics, *Wiley-Interscience publication*, p. 192 and p.1379 (1977)
- [61] P. Pechukas, Distribution of energy eigenvalues in the irregular spectrum, *Phys. Rev. Lett.* **51**, (11), p.943-946 (1983)
- [62] K. Nakamura and M. Lakshmanan, Complete integrability in a quantum description of chaotic systems, *Phys. Rev. Lett.* **57**, (14), p.1661-1664 (1986)
- [63] T. Yukawa, New approach to the statistical properties of energy levels, *Phys. Rev. Lett.* **54**, (17), p.1883-1886 (1985)
- [64] F. Haake, Quantum signatures of chaos, *Springer Verlag*, p.146 and p.363 (2001)
- [65] M. Wilkinson, Narrowly avoided crossings, *J. Phys. A: Math. Gen.* **20**, p.635-645 (1987)
- [66] J. Dorignac and S. Flach, To be published.
- [67] V. V. Ulyanov and O. B. Zaslavskii, Tunneling series in terms of perturbation theory for quantum spin systems, *Phys. Rev. B* **60**, (9), p.6212-6214 (1999)
- [68] It is also possible to compute the first correction to the splitting itself either by using the Rayleigh-Schrödinger perturbation theory applied to each symmetry sectors [66] or by using the Brillouin-Wigner method [67]. We have obtained

$$a_r(q) - b_r(q) = \frac{8}{(r-1)!^2} \left(\frac{q}{4}\right)^r \left[1 - 4\left(\frac{q}{4}\right)^2 \frac{r+2}{(r^2-1)^2}\right].$$

For $r = 1$, the correction to the leading order has to be computed separately. It reads $-q^3/32$. This expression is in exact agreement with the small q expansion of the characteristic values.

- [69] It is interesting to compare this result with the one we may obtain by evaluating the number of states below the separatrix $N_s \simeq 8\sqrt{\alpha}/\pi$, $\alpha \gg 1$ (see (27) in the limit $k \rightarrow 1$). The number of (nondegenerated) pairs of symmetric and antisymmetric eigenstates below the separatrix is thus $n'_c \simeq N_s/2 = 4\sqrt{\alpha}/\pi$ which is very similar to n_c as $8e/\pi \simeq 1.067$. As $E_{N_s} \simeq E_s = 2\alpha$ it proves that expression (20) starts to be valid immediately as $E > E_s$.